Atmos. Chem. Phys., 9, 2499–2517, 2009
www.atmos-chem-phys.net/9/2499/2009/

Atmospheric Chemistry and Physics

A case study of ozone production, nitrogen oxides, and the radical budget in Mexico City

E. C. Wood[1], S. C. Herndon[1], T. B. Onasch[1], J. H. Kroll[1], M. R. Canagaratna[1], C. E. Kolb[1], D. R. Worsnop[1], J. A. Neuman[2], R. Seila[3], M. Zavala[4], and W. B. Knighton[5]

[1]Aerodyne Research, Inc., Billerica, Massachusetts, USA
[2]Earth System Research Laboratory, NOAA, Boulder, Colorado, USA
[3]National Exposure Research Laboratory, Environmental Protection Agency, Research Triangle Park, North Carolina, USA
[4]Molina Center for Energy and the Environment, La Jolla, California, USA
[5]Department of Chemistry and Biochemistry, Montana State University, Bozeman, Montana, USA

Received: 14 July 2008 – Published in Atmos. Chem. Phys. Discuss.: 19 August 2008
Revised: 25 March 2009 – Accepted: 31 March 2009 – Published: 7 April 2009

Abstract. Observations at a mountain-top site within the Mexico City basin are used to characterize ozone production and destruction, nitrogen oxide speciation and chemistry, and the radical budget, with an emphasis on a stagnant air mass observed on one afternoon. The observations compare well with the results of recent photochemical models. An ozone production rate of ∼50 ppbv/h was observed in a stagnant air mass during the afternoon of 12 March 2006, which is among the highest observed anywhere in the world. Approximately half of the ozone destruction was due to the oxidation of NO_2. During this time period ozone production was VOC-limited, deduced by a comparison of the radical production rates and the formation rate of NO_x oxidation products (NO_z). For $[NO_x]/[NO_y]$ values between 0.2 and 0.8, gas-phase HNO_3 typically accounted for less than 10% of NO_z and accumulation-mode particulate nitrate ($NO^-_{3(PM1)}$) accounted for 20%–70% of NO_z, consistent with high ambient NH_3 concentrations. The fraction of NO_z accounted for by the sum of $HNO_{3(g)}$ and $NO^-_{3(PM1)}$ decreased with photochemical processing. This decrease is apparent even when dry deposition of HNO_3 is accounted for, and indicates that HNO_3 formation decreased relative to other NO_x "sink" processes during the first 12 h of photochemistry and/or a significant fraction of the nitrate was associated with the coarse aerosol size mode. The ozone production efficiency of NO_x on 11 and 12 March 2006 was approximately 7 on a time scale of one day. A new metric for ozone production efficiency that relates the dilution-adjusted ozone mixing ratio to cumulative OH exposure is proposed.

Correspondence to: E. C. Wood
(ezrawood@aerodyne.com)

1 Introduction

1.1 Megacities and air pollution

Urban areas are often characterized by the presence of large emissions of pollutants, including volatile organic compounds (VOCs), nitrogen oxides ($NO_x \equiv NO+NO_2$), sulfur dioxide (SO_2), and particulate matter (PM). Many of these compounds (e.g., benzene and diesel PM) are directly toxic to humans (Khan, 2007; McCreanor et al., 2007; Yauk et al., 2008). These primary pollutants react in the atmosphere, forming secondary pollutants such as ozone, formaldehyde, nitric acid, and secondary PM. The spatial distribution of secondary pollutants and their direct effect on public health, vegetation, and the Earth's radiative balance can be quite different than that of their precursor primary pollutants. Ozone (O_3), in particular, plays a central role in tropospheric chemistry, as it is both a product and initiator of photochemistry as well as a potent greenhouse gas. Ozone is one of the US EPA's six criteria air pollutants subject to national ambient air quality standards (NAAQS) created to protect public health. Numerous air basins across the world, spanning urban, suburban, and rural areas, have difficulty meeting relevant air quality standards for O_3. Understanding the formation of O_3 and the transformations of its precursors (VOCs and NO_x) is

Published by Copernicus Publications on behalf of the European Geosciences Union.

crucial for reducing air pollution on both urban and regional scales. Over the past several decades great effort has been focused on characterizing air pollution and atmospheric photochemistry in the US and Europe (Carslaw et al., 2001; Emmerson et al., 2007; Kleinman, 2005; Nunnermacker et al., 1998; Ryerson et al., 2001; Tressol et al., 2008). However, there are few studies of tropospheric photochemistry in developing megacities – where much of the projected increases in population and pollutant emissions over the next several decades are expected to occur (Molina et al., 2004).

During the 2006 MILAGRO (Megacity Initiative: Local And Global Research Observations) campaign, Mexico City was used as a test case for developing megacities. Mexico City is currently the third most populous urban agglomeration in the world, with a population of 19 million (UN, 2008). Although the air quality in Mexico City has improved greatly over the past 10 years (de Foy et al., 2008), it remains highly polluted, with ozone concentrations frequently exceeding 100 ppbv. The motor vehicle fleet, consisting of over 4 million cars and trucks, is older than the US fleet, and approximately 30% of light-duty gasoline vehicles do not have functioning 3-way catalytic converters (CAM, 2008). The latitude (19° 24° N) and altitude of the Mexico City plateau (2.2 km above sea level) leads to elevated actinic flux levels throughout the year. The high altitude also tends to cause fuel-rich combustion in the vehicle fleet.

Inferences about tropospheric photochemistry based on measurements from stationary sites are often complicated by the fact that the observed changes in pollutant concentrations over time are a function of not just chemistry but also meteorology and emissions patterns. Additionally, the air masses observed usually contain a range of aged and fresh pollutants, since primary emission sources of NO_x, VOCs, and PM continue to impact most stationary sites throughout the day. Measurements on board instrumented aircraft are often better suited for tracking the evolution of an air mass over time (Ryerson et al., 2001), though the first 3–7 h of atmospheric oxidation following sunrise usually occur in a shallow boundary layer near the urban surface where it may be unfeasible to fly. Smog chamber studies have provided insight into numerous atmospheric processes, but are challenged by wall interactions and the difficulty in realistically mimicking atmospheric parameters such as actinic flux, low pollutant concentrations, and total atmospheric composition. Some atmospheric processes have not been adequately characterized by laboratory studies, e.g. secondary organic aerosol formation (de Gouw et al., 2005; Volkamer et al., 2006). This emphasizes the importance in quantifying such processes using atmospheric measurements.

In this paper, we present measurements from Pico de Tres Padres, a unique mountain-top stationary site that is situated within the Mexico City basin but is minimally impacted by nearby emissions. The air masses observed on 12 March 2006 were stagnant in the afternoon and provided an excellent opportunity to study ozone chemistry without the confounding influence of transport. Secondary organic aerosol formation at this site is analyzed and described in two related manuscripts (Wood et al., 2009; Herndon et al., 2008). The observations and inferences regarding tropospheric chemistry are compared to the predictions of several photochemical models (Lei et al., 2007; Madronich, 2006; Tie et al., 2007). Such observational-based characterizations of photochemistry, even if focused on a short period of time, are crucial for testing our understanding of the underlying photochemical processes that control secondary air pollution.

1.2 Urban photochemistry overview

Tropospheric ozone is produced by the oxidation of VOCs (volatile organic compounds) in the presence of nitrogen oxides ($NO_x \equiv NO+NO_2$) and sunlight. Central to understanding ozone production is the photostationary state formed between NO, NO_2, and O_3 in sunlight:

$$NO + O_3 \longrightarrow NO_2 + O_2 \quad \text{(R1)}$$

$$NO_2 + h\nu(\lambda < 400\,\text{nm}) \longrightarrow NO + O(^3P) \quad \text{(R2)}$$

$$O(^3P) + O_2 + M \longrightarrow O_3 + M \quad \text{(R3)}$$

Net reaction: null

NO can also be oxidized to NO_2 by compounds other than O_3, most importantly hydroperoxy radicals (HO_2) and organic peroxy radicals (RO_2, where "R" represents an organic group):

$$HO_2 + NO \longrightarrow OH + NO_2 \quad \text{(R4)}$$

$$RO_2 + NO \longrightarrow RO + NO_2 \quad \text{(R5a)}$$

During the day, most of the NO_2 formed from R4 and R5a undergoes photolysis, leading to the creation of ozone (R2 and R3). When discussing ozone production quantitatively, it is useful to use the concept of O_x ("odd-oxygen"), which in the troposphere is often defined as the sum of O_3 and NO_2 ($[O_x] \equiv [O_3]+[NO_2]$). NO_2 is included because it acts as a reservoir of O_3, formed by R1 or as a source of O_3 (R4 and R5a). The sum of the rates of R4 and R5a is therefore equated to the instantaneous production rate of O_x:

$$P(O_x) = \sum_i k_{5ai}[R_iO_2][NO] + k_4[HO_2][NO] \quad (1)$$

Although the right-hand side of Eq. (1) is often defined as $P(O_3)$ (i.e., the instantaneous production rate of O_3 rather than O_x), by defining it as $P(O_x)$ instead there is no need to account for reactions of NO_2 subsequent to its formation, and the expression holds true at all light levels. We note that during the day, typically over 95% of the NO_2 will undergo photolysis to form O_3 (the remainder reacts to form HNO_3 or other compounds), and thus the terms "O_x production" and "ozone production" are often nearly equivalent. However, in the presence of large concentrations of NO, photochemically formed O_x may appear mainly in the form of

NO_2, underscoring the advantage of considering O_x rather than O_3. A more inclusive definition of $[O_x]$ includes $O(^1D)$, $O(^3P)$, NO_3, and N_2O_5, but these compounds are reasonably assumed to be minor contributors to O_x concentrations compared to O_3 and NO_2 during daytime.

In fresh urban plumes with active photochemistry, the production rate of O_x is often much greater than the total rate of the O_x losses, and thus ozone can accumulate in high concentrations (>100 ppbv). O_x is fairly long-lived, with a lifetime range of about a day to weeks.

The sum of NO_x and its oxidation products are known as "reactive nitrogen" or NO_y ($NO_y \equiv NO+NO_2+HNO_3+NO^-_{3(PM1)}$+organic nitrates+$NO_3+2N_2O_5+$ HONO+...), and the oxidation products alone are known as NO_z ($NO_z \equiv NO_y - NO_x$). All NO_z compounds, with the exception of HONO, NO_3, and N_2O_5, are the result of three categories of $RO_x - NO_x$ reactions:

$$RO_2 + NO + M \longrightarrow RONO_2 + M \quad \text{(R5b)}$$

$$NO_2 + OH + M \longrightarrow HNO_3 + M \quad \text{(R6)}$$

$$RO_2 + NO_2 + M \longleftrightarrow RO_2NO_2 + M \quad \text{(R7)}$$

Aerosol nitrate is mainly formed as ammonium nitrate following reaction of HNO_3 with NH_3. In this paper, the products of R5b and R7 are collectively referred to as "organic nitrates", and comprise peroxyacyl nitrates formed from R7 (most commonly peroxyacetyl nitrate, PAN) and multi-functional alkyl nitrates formed from R5b. Partitioning of organic nitrates can form aerosol nitrate as well (Lim and Ziemann, 2005), though the extent to which this occurs in the atmosphere is currently not well quantified.

2 Experimental section

Measurements were made aboard the Aerodyne mobile laboratory, a panel truck outfitted with a suite of real-time instrumentation for gaseous and fine-particulate measurements (Herndon et al., 2005; Kolb et al., 2004). The mobile laboratory was deployed during the MAX/MEX portion of the MILAGRO-2006 campaign to various sites throughout the Mexico City Metropolitan Area (MCMA). Sites were chosen based on the 2–5 day weather forecast and knowledge of how synoptic scale weather patterns typically produce prevailing basin flow archetypes (de Foy et al., 2005; de Foy et al., 2008; Fast et al., 2007). The goal of these deployments was to sample the urban outflow. Some of the mobile laboratory deployment locations are depicted in Fig. 1. Most of the data presented in this manuscript were recorded at Pico de Tres Padres (PTP), which is the highest point in the Sierra de Guadalupe range in the northern section of the MCMA. The sampling altitude at PTP was 720 m above the MCMA valley elevation of 2.2 km. PTP is situated between "T0" and "T1", two of the MAX/MEX supersites

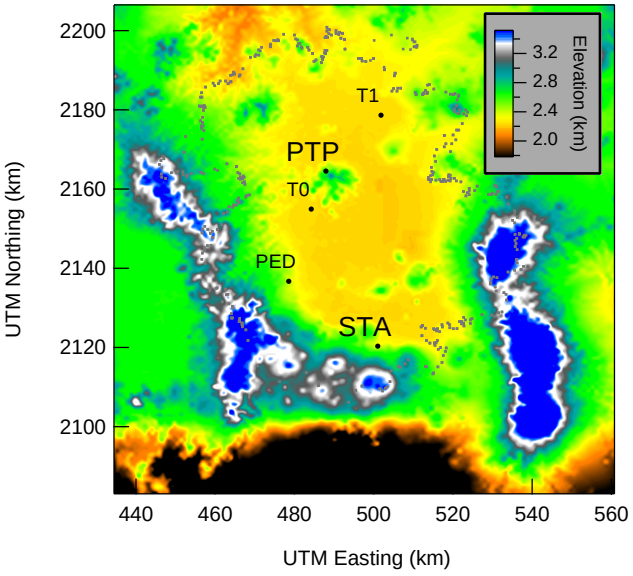

Fig. 1. Selected deployment locations for the mobile laboratory during MILAGRO-2006. The figure is a topographical representation of the Mexico City Metropolitan Area. The sites "T0" and "T1" are the campaign supersites. This work focuses on measurements from Pico de Tres Padres (PTP). Santa Ana (STA) and Pedregal (PED) are the sites of two additional mobile laboratory deployments in the south of the city. The urban core of the federal district is encompassed by T0, PED, and STA. UTM=universal transverse mercator. The border of the *Distrito Federal* is depicted by the grey dots.

(http://www.asp.bnl.gov/MAX-Mex.html) that were hosted by the Instituto Nacional de Petroleo and the Universidad Tecamac, respectively. PTP is ~10 km northeast of T0 and ~19 km southwest of T1.

Nitric oxide (NO) and total reactive nitrogen (NO_y) were measured with a ThermoElectron model 42C chemiluminescence sensor in conjunction with an external molybdenum (Mo) converter that was mounted to the roof of the mobile lab. Measurements of NO were also made with an ECO Physics model CLD 88Y chemiluminescence sensor. Both instruments were periodically calibrated with a standard tank of NO (Scott Specialty gases), diluted with NO_x-free zero air using a ThermoElectron dynamic gas calibrator. The efficiency of the Mo converter for NO_y was quantified by calibrations with NO_2 and n-propyl nitrate. Particulate nitrate was assumed to be converted with the same efficiency as gas-phase species given the high surface area mesh design of the molybdenum converter (Williams et al., 1998). The 1σ uncertainty of the NO 1-min data is the greater of 7% or 0.5 ppbv (NO), and the uncertainty of the NO_y data is estimated as the greater of 15% or 1.5 ppbv. NO_z concentrations were calculated using the NO_y, NO, and NO_2 measurements (i.e., $[NO_z]=[NO_y]-[NO]-[NO_2]$).

Two dual-laser Aerodyne tunable infrared laser differential absorption spectrometers (TILDAS) using pulsed

quantum cascade lasers (Herndon et al., 2007; Nelson et al., 2004) were used to measure NO_2 (at 1606 cm^{-1}), CO (at 2100 cm^{-1}), HCHO (at 1722 cm^{-1}), HNO_3 (at 1721 cm^{-1}), and NH_3 (at 965 cm^{-1}). The inlet for these two instruments consisted of 1 m of heated 1/4" OD PFA tubing followed by a heated teflon-coated cyclone (URG-2000-30ED; aerosol diameter size cut-off of 0.8 μm at a flow rate of 8 liters per minute) and a siloxyl-coated glass orifice to reduce the sampling pressure. The estimated uncertainties for the NO_2, CO, and HCHO measurements are 8%. In order to assess the inlet transmission for $NH_{3(g)}$ and HNO_3, small flows of both gases from permeation tube sources were introduced into the inlet four times. The ambient aerosol loadings (measured with the aerosol mass spectrometer) during these standard additions were in the range 10 to 30 $\mu g/m^3$. The ambient temperature ranged from 16° to 22°C and the relative humidity ranged from 28% to 45%. For comparison, the range of conditions observed between 06:00 and 20:00 LT at PTP was 10° to 27°C and 12% to 75% relative humidity. Inlet losses of NH_3 and HNO_3 were on order 28% and 45% respectively; the measurements have been proportionally corrected. Given the size of the inlet losses and the limited range of ambient conditions under which standard additions were performed, we estimate an uncertainty of 50% for the HNO_3 measurements (the NH_3 measurements are not used quantitatively in this analysis). Only NH_3 and HNO_3 measurements from PTP are included in the analysis.

Ozone (O_3) was measured with a dual-beam absorbance photometer at 254 nm (2B Tech model 205), with an accuracy of 2%. Acetaldehyde, acetone, acetonitrile, benzene, and C3-benzene compounds (sum of C_9H_{12} isomers and C_8H_8O isomers) were measured with a proton-transfer mass spectrometer (Rogers et al., 2006). With the exception of acetonitrile, concentrations were derived from response factors determined from a calibrated gas standard with an accuracy of 25%. Acetonitrile concentrations were determined from transmission corrected ion intensities and equations derived from standard reactions kinetics (Lindinger et al., 1998) assuming a reaction rate constant of 4.74×10^{-9} ml molecule^{-1} s^{-1} (Zhao and Zhang, 2004).

Particulate nitrate (vacuum aerodynamic diameters between 60 and 800 nm–50% cut points) was measured with an Aerodyne compact time-of-flight aerosol mass spectrometer (C-ToF-AMS) with an accuracy of 20% (Canagaratna et al., 2007; Drewnick et al., 2005; Liu et al., 2007). A collection efficiency due to particle bounce of 0.5 was used for all species during the MILAGRO study based on comparisons with other aerosol instrumentation, including a co-located Scanning Mobility Particle Sizer (SMPS; TSI model 3080) and recent laboratory studies (Canagaratna et al., 2007;Matthew et al., 2008). Size distribution measurements from both the AMS and SMPS from this study and previous measurements in Mexico City (Salcedo et al., 2006) indicate that the particulate measurements discussed here represent PM_1 mass loadings.

Thirty-one alkenes were quantified using GC-FID from whole air samples collected in stainless steel canisters (Seila et al., 2001). The alkenes were ethene, propene, 1-butene, trans-2-butene, cis-2-butene, 1-pentene, trans-2-pentene, cis-2-pentene, 1-hexene, 1-heptene, t-3-hexene, 1-octene, t-4-octene, 1-decene, isobutene, 3-methyl-1-butene, 2-methyl-1-butene, 2,4,4-trimethyl-1-pentene, 2-methyl-2-butene, 2,4-dimethyl-1-pentene, 2-methyl-2-pentene, 1,3-butadiene, cyclopentene, cyclooctene, cyclohexene, isoprene, limonene, camphene, beta pinene, and alpha pinene.

Photolysis rate constants for O_3, HCHO, acetaldehyde, and acetone were determined by a combination of measurement and model results. The photolysis rates calculated from the Scanning Actinic Flux Spectroradiometer operated by B. Lefer and J. Flynn at the T1 site were used in conjunction with the NCAR tropospheric ultraviolet and visible radiation model (TUV). Equation (2) was used to estimate photolysis rates: $j_{PTP} = \frac{j_{PTP}(TUV)}{j_{T1}(TUV)} \times j_{T1}$(measured) (2)where j_{PTP}(TUV) and j_{T1}(TUV) are the model results and j(measured) is from the T1 measurement. This approach uses TUV to account for the difference in elevation between PTP and T1 (850 m), for which aerosol and absorbing gases affect the optical transmission. The hourly vertical profiles of ozone used in the model were generated from the measurements at T0 and PTP. Although no information regarding the NO_2 and O_3 column above the convective mixing layer was included, the systematic errors associated with this are expected to cancel in the first factor of the right-hand side of Eq. (2). The total ozone column is characterized by the T1 measurements. The ratio of j_{PTP}(TUV)/j_{T1}(TUV) depends on the specific molecular photolysis rate, but for all of the compounds discussed in this work, the altitude correction is less than 16%.

The largest source of uncertainty in the photolysis rate constants by this approach lies in the fact that PTP is ~19 km away from T1 and the cloud cover was not spatially identical. A comparison of the measured radiometer data at T1 and an Eppley UV photometer used aboard the mobile laboratory suggests qualitative agreement when cloud patches moved above the region. For the periods in which the photolysis rates were analyzed, there was minimal cloud cover (i.e., it was not cloudy).

A second source of uncertainty in this approach stems from the differences in albedo and upwelling/downwelling radiation associated with the elevation and topographical differences between T1 and PTP. The T1 measurement data is based on the downwelling radiation, however at PTP the photolysis rate in the sampled air had a contribution from reflected light. We estimate that this contributes an uncertainty of 4% in the calculated photolysis rates, based on the average Mexico City albedo.

Additional sources of error in this approach are due to the absence of modeled absorbers in the 850 m elevation distance between T1 and PTP. Hourly profiles of ozone and NO_2 were used in the model, though SO_2, HONO, HCHO

and acetaldehyde were ignored. The bias introduced by neglecting these absorbers would result in an underestimate of the photolysis rates at PTP since such absorption leads to higher photolysis frequencies at higher altitudes. This underestimate is likely most pronounced in the early morning when the convective mixing layer height is below the altitude of PTP.

The combined uncertainties in the photolysis rates (accounting for the altitude, cloud coverage, albedo, and unknown absorbers) is estimated as 25%.

All stated accuracies reflect 1σ uncertainty. All reaction rate constants used are those from the latest JPL recommendations (Sander et al., 2006). One-minute averages are used for all measurements presented, with the exception of the VOC canister measurements which were 30 min averages. The NO_2 data are one minute averages recorded every three minutes, thereby affecting the O_x and NO_z values too. All linear correlation fits were calculated using a least-squares algorithm that accounts for the uncertainty in both variables.

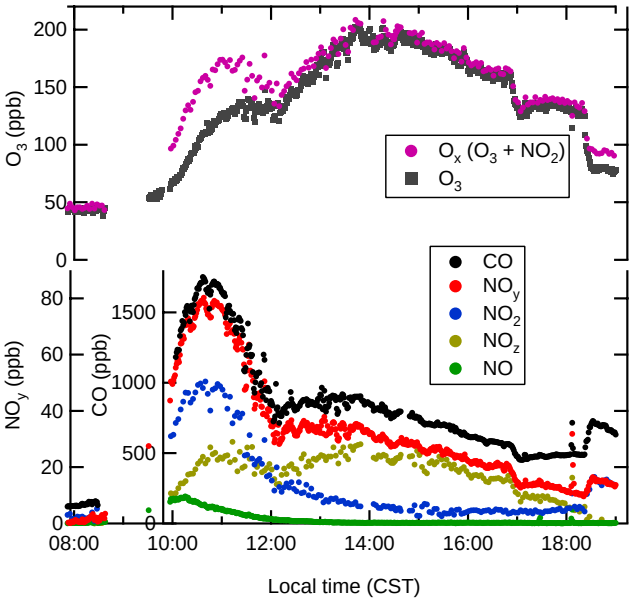

Fig. 2. Time series of several species at PTP on March 12, 2006. The time period between 12:15 and 13:15 was characterized by stagnant air and is used to infer the production rates of O_x and NO_z. The gap in the data between 08:30 and 10:00 is due to instrument maintenance.

3 Results and discussion

3.1 Air masses observed at PTP

Because the mobile laboratory payload did not include any direct measurements of the vertical structure of the atmosphere, the measurements of the convective mixing layer heights at T0 and T1 (Shaw et al., 2007) have been examined as a proxy. Typically, during clear-sky insolation, the mixed layer grew to a height of ∼1 km above T0 by 11:30 local time (LT). CO mixing ratios increased sharply at PTP near 09:30. That pollution reached PTP before the mixing layer height reached the elevation of PTP (as measured at T0 and T1) is most likely due to differential heating and upslope winds.

The altitude and horizontal location within the city and the lack of short "spikes" in the time series of all species indicate that PTP was not greatly affected by nearby emissions, and thus was a near-ideal stationary measurement location for sampling mixed urban emissions during their first 2 to 12 h of photochemistry. This is in contrast to most ground sites within cities, which are usually close (within 100 m) to traffic and other pollution sources. Based on the measured wind speeds, the emissions from the closest neighborhood (∼4 km to the south) would have had on the order of 15–60 min to mix into the urban plume. On 12 March 2006 (the day highlighted in this work), the transport time from other parts of the city was on the order of 1–5 h, whereas vertical mixing time scales in the afternoon are typically less than 30 minutes (Stull, 1988). Therefore, as the mixing layer grew above PTP, the sampled air masses were typically an accumulation of pollutants from many sectors of the city mixed both vertically and horizontally over several hours. Multi-day accumulation of pollutants is rare in Mexico City due to efficient venting (de Foy et al., 2006).

PTP was above the nocturnal boundary layer during most of each night. With the exception of a few episodes in which fresh emissions were brought to the site by strong winds or when trapped residual layers advected past the site, the nighttime measurements were indicative of a clean residual boundary layer. For example, the mean nighttime mixing ratios of CO, O_3, NO_y and CH_3CN (acetonitrile) between 02:00 and 06:00 on 12 March were 132, 44, 0.6, and 0.2 ppbv, respectively. The organic aerosol loading at night was 1.1 $\mu g\,m^{-3}$ (STP, 273 K and 1 atm) and was highly oxidized.

Much of this work focuses on data from 12 March 2006, in which there was a one-hour pause in the rise of the mixing layer in the afternoon. Figure 2 shows a time series of CO, O_3, O_x, NO_y, NO, NO_2, and NO_z concentrations observed at PTP on Sunday, 12 March 2006. Concentrations of all species rose sharply starting at ∼09:00 CST, as upslope winds transported pollutants from below the sampling elevation to PTP. Concentrations of CO (which is relatively photochemically inactive) reached an initial peak at 10:40 due to upslope winds, though the mixing layer depth at T0 did not reach the elevation of PTP (720 m above the city elevation) until ∼11:30 as described earlier. [CO] decreased between 11:00 and 12:00 as the mixing layer rose above PTP and the effect of dilution overweighed the flux of CO from below.

The measurements of the convective mixing depth above T0 show no increase between 12:00 and 13:00 on 12 March 2006 (Shaw et al., 2007). The urban emission inventory (CAM, 2008), which apportions on-road emissions by hour of day, indicates that the amount of CO emitted between 12:00 and 13:00 is equal to 15% of the amount emitted between 05:00 and 12:00. This should lead to an increase of [CO] by approximately 15% above the background mixing ratio if there is no mixing with the residual layer aloft caused by a rising boundary layer. The observed enhancement in [CO] between 12:15 and 13:15 was 14% (calculated as $([CO]_{13:15}-130\,ppbv)/([CO]_{12:15}-130\,ppbv)$ to account for the background CO mixing ratio of 130 ppbv). The favorable comparison between the observed and predicted increase in [CO] complements the T0 measurements showing a pause in the rise of the mixing layer between 12:15 and 13:15. This analysis is not sensitive to inaccuracies in the absolute magnitude of CO emissions; it is sensitive only to the reported *timing* of CO emissions between the early morning and afternoon, since the quantity used is the relative increase in [CO] rather than the absolute mixing ratios. This time period was unlike most other days at PTP, when boundary layer dynamics and advection played much greater roles in determining changes in pollutant concentrations.

A comparison of the ratios of several primary pollutants at PTP and T0 (a site greatly impacted by fresh urban emissions) indicates that the air observed at PTP was representative of mainly urban emissions and was not greatly affected by biomass burning, biogenic VOCs, or other non-urban pollutants. The $\Delta[NO_y]/\Delta[CO]$, Δ[benzene]/Δ[CO], and $\Delta[CH_3CN]/\Delta[CO]$ ratios were deduced from linear fits of the correlation graphs of 1-min data. The $\Delta[NO_y]/\Delta[CO]$ ratio was 0.050 ppbv/ppbv (R = 0.99) on 11 and 12 March, 0.054 ppbv/ppbv (R=0.95) for the entire PTP dataset, and between 0.04 and 0.07 ppbv/ppbv at T0. The Δ[benzene]/Δ[CO] ratio was 1.8 pptv/ppbv (R=0.93) on 11 and 12 March 2006, 1.67 pptv/ppbv (R=0.87) for the entire PTP dataset, and 1.1 to 1.8 at T0. The $\Delta[CH_3CN]/\Delta[CO]$ ratio on 12 March 2006 was between 0.2 to 0.5 pptv/ppbv. Other measurements in urban air have been in the range 0.1–0.3 (Kleinman et al., 2008; Knighton et al., 2007), while the ratios observed in air impacted by biomass burning are between 1 and 7 (de Gouw et al., 2006). This suggests that biomass burning probably did not have a significant impact on the air on 12 March until 18:00, when a biomass burning PM plume was observed. Isoprene (canister) and other biogenic VOCs (e.g., terpenes) typically accounted for less than 10% of the calculated VOC reactivity over the entire PTP dataset, indicating there was only a small influence from biogenic emissions.

3.2 O_x production and loss rates

Given the well-characterized, stagnant meteorology of 12 March 2006, the measurements are used to characterize numerous aspects of tropospheric chemistry. The average wind speed during this time period was 1.5 m/s from the southeast, so the air sampled spanned less than a 6 km horizontal range – most of which is unpopulated land along the mountain slope, with no urban emission sources. For comparison, the distance between T0 and PTP is ~10 km. Other days were excluded from this analysis because of at least one of the following two filtering criteria: 1) the wind speeds were greater than 2 m/s, and 2) [CO] did not show a gradual increase of less than 100 ppbv/h in the afternoon as observed on 12 March. On most other days, [CO] steadily decreased in the afternoon as the mixing depth grew above PTP.

Table 1. Quantification of the destruction (loss) rate of O_x between 12:15 and 13:15 on 12 March 2006. Mixing ratios used for these calculations: $[O_3]$=160 ppb (measured), $[H_2O]$=7 ppth (measured), $[HO_2]$=40 ppt (estimated), $[OH]=6\times10^6$ molec/cm^3 (estimated). A boundary layer height of 0.9 km and a deposition velocity of 0.4 cm/s were used to calculate the dry deposition rate of O_3. The oxidation rate of NO_2 was calculated as $0.8\times P(NO_z)$.

Reaction	Rate (ppbv/h)
$O(^1D)+H_2O$	1.0
HO_2+O_3	0.8
$OH+O_3$	0.2
$NO_2\rightarrow NO_z$	6.0
O_3+VOCs	0.7
O_3 dry deposition	2.6
$NO_3+h\nu\rightarrow NO+O_2$	0.3
Total	11.6

We assume that concentrations of O_x and NO_z were both vertically homogeneous within the mixing layer and horizontally homogeneous within the ~5.4 km air mass sampled during this hour. From 12:15 to 13:15 we interpret the observed increases in $[O_x]$ and $[NO_z]$ to be mainly due to photochemistry, with an estimated uncertainty of 25% due to the coarse level of knowledge regarding the mixing layer depth and the assumption of horizontal homogeneity for $[O_x]$ and $[NO_z]$.

Given these assumptions, the average O_x production rate $P(O_x)$ during this time is estimated using the observed time rate of change of O_x ($\Delta[O_x]/\Delta t$; t ≡ time) and the calculated O_x loss (destruction) rate $L(O_x)$ according to Eq. (2):

$$\Delta[O_x]/\Delta t = P(O_x) - L(O_x) \quad (2)$$

where the sign of $L(O_x)$ is positive. The value of $\Delta[O_x]/\Delta t$ is 37 ppbv/h, calculated from the time series data. $L(O_x)$ is calculated from R6–R7 and R8–R15 as summarized in Table 1:

$$L(O_x) = \Sigma \text{ Rates (R6, R7, R8 to R15)} \quad (3)$$

$$O_3 + h\nu \longrightarrow O(^1D) + O_2 \quad \text{(R8)}$$

$$O(^1D) + H_2O \longrightarrow 2OH \quad \text{(R9)}$$

$$HO_2 + O_3 \longrightarrow OH + 2O_2 \quad \text{(R10)}$$

$$OH + O_3 \longrightarrow HO_2 + O_2 \quad \text{(R11)}$$

$$O_3 + \text{VOCs} \longrightarrow \text{products} \quad \text{(R12)}$$

$$NO_2 + O_3 \longrightarrow NO_3 + O_2 \quad \text{(R13)}$$

$$NO_3 + h\nu \longrightarrow NO + O_2 \quad \text{(R14)}$$

O_3 dry deposition (R15)

The NO_z production rate is used to quantify O_x losses from R6 and R7 because the products of these two reactions form observable NO_z species. Because these two reactions account for approximately 80% of total NO_z production (based on the NO_y speciation observed at the T1 site (Farmer et al., 2009), O_x loss by R6 and R7 is calculated from the observed NO_z production rate (Sect. 3.3.1) multiplied by 0.8. The rates of R10 and R11 are calculated assuming an HO_2 mixing ratio of 40 pptv and an OH concentration of 6×10^6 molecules cm^{-3} (as estimated later in this section and in section 3.3.3). Alkene measurements were not available on the afternoon of 12 March, and so the rate of alkene ozonolysis (R12) is based on measurements from other afternoons at PTP that had similar concentrations of CO, O_3, and aromatic VOCs (which were measured continuously by the PTR-MS). O_x destruction via the minor NO-yielding branch of NO_3 photolysis was calculated assuming that NO, NO_2, and NO_3 were in a photostationary state (Geyer et al., 2003). Dry deposition of O_3 was estimated using the boundary layer height of 0.9 km and a deposition velocity of 0.4 cm s^{-1} (Wesely and Hicks, 2000).

As seen in Table 1, the single greatest loss mechanism of O_x was the conversion of NO_2 into NO_z compounds, which accounted for approximately 50% of O_x destruction. The importance of NO_2 oxidation as an indirect O_3 sink likely decreased after one day of photochemistry, since most NO_x is converted to NO_z on this time scale. The other O_x destruction mechanisms are not expected to change as greatly after one day. The relative importance of ozone photolysis (R8 and R9) as an O_x sink during the entire 11-day PTP data set depended greatly on the meteorology, since the rate is proportional to the mixing ratio of water vapor.

With the value of 12 ppbv/h for $L(O_x)$ as described above, the O_x production rate is calculated using Eq. (3) as 49±15 ppbv/h, in which the uncertainty is based on the uncertainty in the fit of the slope of the time series data as well as uncertainty in the mixing layer depth.

Primary emissions of NO_2 are estimated to account for less than 1% of observed O_x at all times at PTP as estimated by the quantity $0.04[NO_y]/[O_x]$, where the average NO_2/NO_x emission ratio in Mexico City is assumed to be 4%. This emission ratio is an upper limit based on early-morning measurements of NO, NO_2, and O_3 at the T0 site (near urban emissions) and previously published literature values (Shorter et al., 2005). Net thermal decomposition of peroxyacyl nitrates would act as a source of O_x as well, but it is not evident from our measurements whether there was net formation or decomposition of peroxyacyl nitrates during the afternoon at PTP. We estimate that an upper limit to the contribution of peroxyacyl nitrate thermal decomposition to O_x production during the stagnant period was 2 ppbv/h.

The inferred $P(O_x)$ value of 49±15 ppbv/h agrees within 50% with $P(O_x)$ calculations based on the VOC reactivity and estimated OH concentrations (Wood et al., 2009). Ozone production rates calculated using measurements of HO_2 and NO and Eq. (1) reached even higher values of up to 100 ppbv/h in the afternoon at more centrally-located urban site in Mexico City (Dusanter et al., 2009; Shirley et al., 2006). These values are among the highest observed anywhere in North America. A comparison of ozone production rates in Phoenix, Philadelphia, and Houston (Kleinman et al., 2002) indicated peak ozone production rates of approximately 5, 16, and 20 ppbv/h, respectively, with elevated rates of over 50 ppbv/h observed in petrochemical plumes in Houston. Peak instantaneous ozone production rates of 30–36 ppbv/h have been observed in Nashville (Daum et al., 2000; Thornton et al., 2002). The VOC reactivity at PTP calculated as $\Sigma k_{OH+VOC}[VOC]$ was extremely high compared to the other locations – measurements from the afternoon of 11 and 12 March ranged from 13 s^{-1} to 20 s^{-1}. In comparison, the 90th percentile VOC reactivities in Nashville, Phoenix, and Houston were 6 s^{-1}, 5 s^{-1}, and 22 s^{-1}, respectively (Kleinman et al., 2002). The calculated VOC reactivities at PTP are in rough agreement with measurements of the total OH loss rate in Mexico City in 2003 (Shirley et al., 2006) of ∼25 s^{-1} in the afternoon – approximately 80% of which was due to reaction with VOCs and CO (i.e., the VOC reactivity was approximately 20 s^{-1}). A quantitative discussion of the speciated VOC reactivity at PTP and T0 is presented in Wood et al. (2009).

Given the NO mixing ratio of 1.0±0.5 ppbv between 12:15 and 13:15, we estimate that the sum of $[HO_2]$ and $[RO_2]$ was 95±50 pptv using Eq. (1) and the rate constant of R4 (8.1×10^{-12} cm^3 $molecule^{-1}$ s^{-1}) for oxidation of NO by RO_2. Observations aboard the C-130 aircraft at comparable NO_x concentrations (>10 ppbv) have shown that HO_2 comprised slightly less than 50% of the sum of HO_2 and RO_2 (Cantrell et al., 2007). This value is useful for estimating the rate of the HO_2 self-reaction and the rate of HO_2+O_3. The large uncertainties do not affect the conclusions of this paper.

3.3 Nitrogen oxides

3.3.1 Production rateof NO_z

The value of $P(NO_z)$ can be inferred using a method similar to that used to infer $P(O_x)$ in Sect. 3.2 (i.e. $\Delta[NO_z]/\Delta t = P(NO_z) - L(NO_z)$). The value of $\Delta[NO_z]/\Delta t$

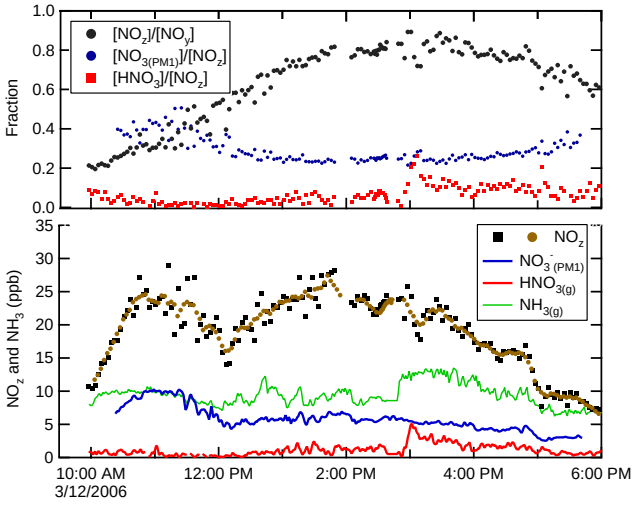

Fig. 3. Partial speciation of NO_y at PTP. The NO_z data are depicted both as 3 minute averages (black squares) and as smoothed, 12 minute running averages (brown circles). Particulate nitrate ($NO^-_{3(PM1)}$) accounts for 20-40% of NO_z during the day, and $HNO_{3(g)}$ accounts for less than 10%. Gaseous NH_3 is included for comparison, though is not a part of NO_y or NO_z.

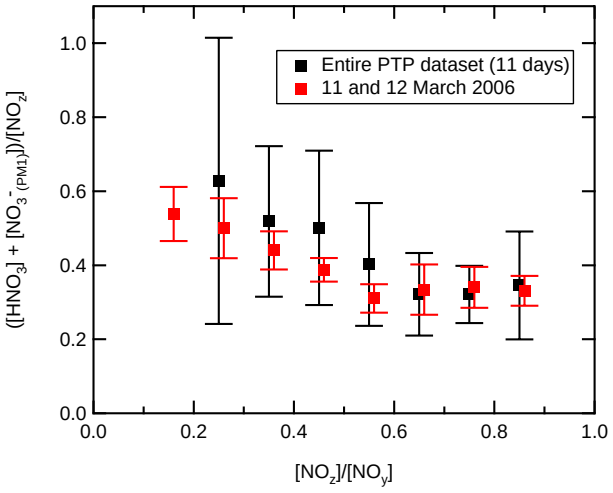

Fig. 4. Speciation of NO_z as a function of $[NO_z]/[NO_y]$. Mean values of $([HNO_3] + [NO^-_{3(PM1)}])/[NO_z]$ using the entire PTP dataset and 11-12 March 2006 between 8:00 and 20:00 are displayed in $[NO_z]/[NO_y]$ bins of width 0.1 Error bars are ± one standard deviation of the 1-min averaged values.

between 12:15 and 13:15, calculated as $([NO_z]_{12:15}-[NO_z]_{13:15})/1$ h), was 6.8±1.7 ppbv/h. Losses of NO_z during this time period can be constrained by the observed decrease in $\Delta[NO_y]/\Delta[CO]$, calculated as $([NO_y]–0.6)/([CO]–130)$ (i.e., the background-adjusted $[NO_y]$:[CO] ratio). Since CO is relatively unreactive on a time scale of hours, it is useful as a dilution tracer. During the stagnant hour, $\Delta[NO_y]/\Delta[CO]$, decreased by only 6%. If the overall urban $[NO_x]/[CO]$ emission ratio did not change enough to affect the ratio of cumulative (integrated) NO_x and CO emitted, and if the decrease in $[NO_y]/[CO]$ was solely due to NO_z losses rather than NO_x losses, then this 6% decrease in $[NO_y]/[CO]$ would correspond to a 9% decrease in NO_z, since $[NO_z]/[NO_y]$ was on average 0.65. The assumption regarding the changes in the overall urban NO_x/CO emission ratio is supported by the 2006 emission inventory (CAM, 2008) and discussed further in Sect. 3.3.2. Thus we calculate that $P(NO_z)$ is 9% higher than $\Delta[NO_z]/\Delta t$ and equal to 7.4±1.9 ppbv/h.

3.3.2 Speciation of NO_y

Between 12:15 and 13:15, $[NO_x]/[NO_y]$ decreased from 0.5 to 0.2 due to the oxidation of NO_x into NO_z compounds (Fig. 3). The speciation of NO_z can only partially be described since our directly measured individual NO_z species were restricted to accumulation-mode particulate nitrate ($NO^-_{3(PM1)}$) and gas-phase HNO_3. Particulate nitrate comprised 40% of NO_z from 10:00 to 11:00 (Fig. 3) and decreased to approximately 22% by 13:00. Nitric acid accounted for less than 4% of NO_z until 15:00, when it increased to 12%. The sum of $[HNO_{3(g)}]$ and $[NO^-_{3(PM1)}]$, henceforth referred to as ΣNO^-_3, accounted for 43% of NO_z in the morning and decreased to a minimum value of 25% shortly before 15:00.

Since the $NO^-_{3(PM1)}$ measurement only accounts for accumulation mode nitrate (vacuum aerodynamic diameter less than 1 μm), any uptake of NO_y onto coarse-mode PM is not accounted for in this speciation. The dominant mode peak of the $NO^-_{3(PM1)}$ size distribution was 330 nm at 10:00 and increased to 380 nm by 12:00. The same trend was observed in the ammonium aerosol size distributions.

The partitioning of $HNO_{3(g)}$ and $NO^-_{3(PM1)}$ at other ground sites in Mexico City has been described recently (Fountoukis et al., 2007; Hennigan et al., 2008; San Martini et al., 2006; Zheng et al., 2008). The high NH_3 mixing ratios act to drive photochemically formed HNO_3 into particulate ammonium nitrate (NH_4NO_3). As the temperature increases in the afternoon, NH_4NO_3 vaporizes, releasing HNO_3 vapor and increasing the ratio of $HNO_{3(g)}$ to $NO^-_{3(PM1)}$ (Fountoukis et al., 2007; Hennigan et al., 2008; Zheng et al., 2008).

The relative partitioning of NO_z among HNO_3, NO^-_3, and other compounds not measured at PTP (e.g., peroxyacyl nitrates, alkyl nitrates, and coarse-mode nitrate PM) is determined by the net production and loss rates of the main NO_z species (R6 – R7). Figure 4 shows that $[\Sigma NO^-_3]/[NO_z]$ decreases with photochemical processing (i.e., with increasing $[NO_z]/[NO_y]$). Figure 4 shows the means and standard deviations of the 1-minute averaged data from 12 March 2006 and the entire 11-day PTP dataset between 08:00 and 16:00, which spans a range of meteorological conditions. This overall trend agrees with measurements aboard the C-130 aircraft in which the sum of $HNO_{3(g)}$ and $NO^-_{3(PM1)}$ (as measured by an AMS) accounted for 30%–40% of NO_z in aged

air masses ($[NO_z]/[NO_y]>0.7$) (Flocke, personal communication, 2008). Speciated NO_y measurements at the T1 site exhibited similar trends (Farmer et al., 2009).

We discuss three possible factors contributing to the observed decrease in $[\Sigma NO_3^-]/[NO_z]$: 1) Deposition of $HNO_{3(g)}$, 2) A decrease in the role of HNO_3 formation relative to total NO_z formation, and 3) a shift of the nitrate aerosol size distribution from the accumulation mode to the coarse mode (particles greater than 1 μm in diameter), which is not detected by the AMS.

The first possible explanation of the decrease in $[\Sigma NO_3^-]/[NO_z]$ with photochemical age is enhanced deposition of HNO_3 relative to the other NO_z compounds. Gas-phase HNO_3 has a high dry deposition velocity (Wesely and Hicks, 2000), but the fact that the high NH_3 concentrations present in Mexico City convert most HNO_3 into particulate ammonium nitrate (Hennigan et al., 2008) suggests that this effect may not be as important as it is in low NH_3 environments. The extent to which HNO_3 deposition caused the decrease in $[\Sigma NO_3^-]/[NO_z]$ can be constrained by the small decreases observed in $\Delta[NO_y]/\Delta[CO]$ over the course of each day. Over the entire PTP dataset between 08:00 and 18:00, $\Delta[NO_y]/\Delta[CO]$ decreased from a median value of 0.050 at $[NO_z]/[NO_y]$ values less than 0.2 (during the morning) down to 0.045 at $[NO_z]/[NO_y]$ values greater than 0.6 (which occurred on some but not all afternoons). If this decrease in $[NO_y]/[CO]$ is assumed to be due solely to deposition of HNO_3 and $NO_{3(PM1)}^-$, then the observed values of $[\Sigma NO_3^-]/[NO_z]$ can be "corrected" upwards to account for this deposition as described in Sect. 3.3.1. Such a correction is complicated by the fact that the NO_x:CO emission ratio is not constant throughout the day. The key quantity that must be considered is the ratio of *cumulative* NO_x emissions to *cumulative* CO emissions. The emissions inventory (CAM, 2008) indicates that this ratio varies by less than 10% after 09:00. Overall, the value of $[\Sigma NO_3^-]/[NO_z]$ can be increased by at most a factor of 1.2 to account for HNO_3 deposition. This does not explain the overall decreasing trend in $[\Sigma NO_3^-]/[NO_z]$ observed with increasing photochemical age.

The second possible explanation for the decrease in $[\Sigma NO_3^-]/[NO_z]$ over time is that there was a decrease in the HNO_3 production rate relative to that of the other unmeasured NO_z compounds, presumably peroxyacyl nitrates (R7) and multifunctional alkyl nitrates (R5b). The equilibrium constant for R7 for many organic peroxy radicals (such as the peroxyacetyl radical, $CH_3C(O)O_2$) is very sensitive to temperature, and the corresponding peroxyacyl nitrates can either be in a state of net formation or net thermal decomposition depending on temperature and the concentrations of the relevant species. The lack of knowledge of the peroxyacyl nitrate mixing ratios themselves combined with the uncertainties in the mixing ratios of OH, NO, NO_2, and the precursor compounds (e.g., acetaldehyde for peroxyacetyl nitrate) preclude a quantitative assessment of whether peroxyacyl nitrates were undergoing net formation or net decomposition during the stagnant hour. We note that the results of one modeling study (Lei et al., 2007) showed that there was net formation of PAN compounds during the day in Mexico City, though not necessarily under the same conditions observed at PTP. Similarly, a box-model study of the Mexico City outflow indicated that the ratio of the production rate of HNO_3 to the net production rate of total PAN compounds decreases in the early afternoon of the first day of photochemistry (Madronich, 2006), though the temperature was held at 10°C in the model. The thermal decomposition lifetime (1/e) of PAN varies from ~1 h at 24°C to 2 days at 0°C.

The third possible explanation for the observed decrease in $[\Sigma NO_3^-]/[NO_z]$ with increasing $[NO_z]/[NO_y]$ is that there was a shift in the size distribution of aerosol nitrate from the accumulation mode (where it can be detected by the AMS) to the coarse mode (Laskin et al., 2005). The AMS is most sensitive to particles with vacuum aerodynamic diameters between ~60 nm and ~800 nm (Canagaratna et al., 2007), whereas the NO_y (and NO_z) measurements do not have a particle size cut-off. This is a plausible explanation, especially since coarse-mode nitrate has been observed in Mexico City during MILAGRO (Moffet et al., 2008; Querol et al., 2008), however it cannot be quantified using the PTP dataset as there was no measure of the coarse mode particulate nitrate mass. The decrease in the accumulation mode nitrate mass during the morning is consistent with increasing ambient temperature and the associated shift in the ammonium nitrate equilibrium (Zheng et al., 2008). On 11 and 12 March, the AMS (and SMPS) mass distribution data indicated an increase in the particulate nitrate mass mode from 330 nm to 380 nm between 10:00 and 12:00. This shift in the aerosol size distribution increased the fraction of total mass in particles greater than 800 nm to which the AMS is less sensitive, which may also have contributed to the observations.

In summary, the decreasing trend in $[\Sigma NO_3^-]/[NO_z]$ with photochemical age displayed in Fig. 4 cannot be fully explained by deposition of $HNO_{3(g)}$, and was likely caused by some combination of a decrease in the production rate of HNO_3 relative to other NO_z compounds, a shift of the nitrate aerosol mass distribution from the accumulation mode to the coarse mode, and a shift of the accumulation mode mass distribution toward particles greater than 800 nm (vacuum aerodynamic diameter). Similar conclusions regarding the importance of deposition and coarse-mode nitrate were reached in Zheng et al. (2008).

3.3.3 Estimate of OH

The increase in $[\Sigma NO_3^-]$ during the stagnant period can be used to infer the average OH concentration since ΣNO_3^- is the result of R6 and $[NO_2]$ was measured. Between 12:15 and 13:15, $[\Sigma NO_3^-]/\Delta t$ was 1.9±0.5 ppbv/h, which is approximately 30%±8% of the total increase in NO_z. Given

the average NO_2 mixing ratio of 10 ppbv and the rate constant for R6, the average OH concentration during the stagnant period is estimated as 6×10^6 molecules cm^{-3}, which is in line with previous afternoon measurements of OH in Mexico City (Shirley et al., 2006). This value is an underestimate of [OH] if there was an increase in coarse-mode nitrate (and low by a factor of $(HNO_{3(g)}+NO^-_{3total})/(HNO_{3(g)}+NO^-_{3PM1})$). Conversely, this is an overestimate of [OH] if HNO_3 was not the sole source of particulate nitrate (i.e., if there was significant partitioning of organic nitrates to the condensed phase). Besides the comparison to previous measurements of OH in Mexico City, this estimate of [OH] is only used to quantify the rates of R11 and R19. The uncertainty in this estimate does not affect the conclusions presented. For example, this estimate would have to be more than a factor of 6 too low in order for R11 to account for an appreciable fraction (>10%) of the total O_x loss.

3.4 Radical budget and ozone production

The photochemistry of ozone production and atmospheric oxidation in general is driven by RO_x ($RO_x \equiv OH+HO_2+RO_2$) radicals. The design of effective air pollution abatement strategies requires knowledge of whether ozone production is "NO_x-limited" or "VOC-limited" (NO_x-saturated), which is intimately related to reactions between RO_x and NO_x. At low NO_x mixing ratios, self-reactions of RO_x (R16–R19) dominate the removal processes of RO_x, the O_x production rate increases with increasing NO_x concentration, and O_x production is NO_x-limited. At higher NO_x concentrations, reactions with NO_x dominate the RO_x removal processes, the O_x production rate decreases with increasing NO_x concentrations, and O_x production is VOC-limited.

In order to investigate the radical budget and to determine whether ozone production was NO_x-limited or VOC-limited during the afternoon of 12 March, we compare the NO_z production rate described in Sect. 3.3.1 to the production rate of RO_x radicals. The reactions of RO_x with NO_x are the same reactions that form NO_z, i.e. formation of HNO_3, $RONO_2$, and RO_2NO_2 compounds (R5b, R6, R7). Thus the observed NO_z production rate serves as an indicator of the sum of the rates of R5b, R6, and R7. RO_x sinks not accounted for by $P(NO_z)$ are from RO_x self-reactions:

$$HO_2 + HO_2 \longrightarrow H_2O_2 + O_2 \quad \text{(R16)}$$

$$RO_2 + HO_2 \longrightarrow ROOH + O_2 \quad \text{(R17)}$$

$$RO_2 + RO_2 \longrightarrow \text{products} \quad \text{(R18)}$$

$$OH + HO_2 \longrightarrow H_2O + O_2 \quad \text{(R19)}$$

In steady state, the production rate of RO_x ($P(RO_x)$) equals the loss rate of RO_x ($L(RO_x)$). Since all losses of RO_x by reaction with NO_x form observable NO_z species (R5b–R7), $P(RO_x)$ is equal to $P(NO_z)$ when ozone production is strongly VOC-limited (Eq. 3):

$$P(RO_x) = L(RO_x) \approx P(NO_z) \quad (4)$$

whereas $P(NO_z)$ is much less than $P(RO_x)$ when ozone production is NO_x-limited. Thus a comparison of $P(RO_x)$ and $P(NO_z)$ serves as a useful indicator of whether ozone production is NO_x-limited or VOC-limited. Note that $P(NO_z)/P(RO_x)$ is similar to the "L_N/Q" quantity used by Kleinman et al. (2005).

The validity of Eq. (3) assumes that all observable NO_z compounds are formed by RO_x-NO_x reactions. The only observable NO_z species that are not formed by RO_x-NO_x reactions according to the current understanding of NO_y chemistry are NO_3, N_2O_5, and heterogeneously-formed HONO, and it is unlikely that any of these compounds accounts for an appreciable fraction of NO_z during the day.

In order to compare $P(RO_x)$ and $P(NO_z)$, we calculate $P(RO_x)$ from the following RO_x sources for the PTP data set: reaction of $O(^1D)$ with water vapor (R8 and R9); photolysis of the oxygenated VOCs formaldehyde, acetaldehyde, and acetone (R20–R22); and ozonolysis of alkenes (R23):

$$HCHO + h\nu + 2O_2 \longrightarrow CO + 2HO_2 \quad \text{(R20)}$$

$$CH_3CHO + h\nu + 2O_2 \longrightarrow CH_3O_2 + HO_2 + CO \quad \text{(R21)}$$

$$CH_3COCH_3 + h\nu + 2O_2 \longrightarrow CH_3C(O)O_2 + CH_3O_2 \quad \text{(R22)}$$

$$O_3 + \text{alkenes} \longrightarrow \text{products} + RO_2 + OH \quad \text{(R23)}$$

RO_x yields for alkene-ozonolysis reactions are based on the tabulated OH yields of Calvert et al. (2000) and are doubled to account for co-generated peroxy radicals.

The time series of these photolytic RO_x sources for 12 March 2006 is depicted in Fig. 5. The average value of $P(RO_x)$ from the reaction of $O(^1D)$ with water vapor and the photolysis of oxygenated VOCs between 12:15 and 13:15 was 1.3 ± 0.4 pptv/s. VOC canister measurements were not made during this time period, and so the contribution of alkene ozonolysis to $P(RO_x)$ is not accurately known. This quantity is estimated as 0.4 ± 0.2 pptv/s, based on the ozonolysis rates calculated from other afternoon samples at PTP with comparable values of concentrations of O_3, CO, aromatic VOCs, and photochemical age values calculated using a C3-benzene photochemical clock (Herndon et al., 2008). The total calculated $P(RO_x)$ is therefore 1.7 ± 0.5 pptv/s, with the range reflecting the uncertainty in the contribution from alkene ozonolysis and the uncertainty in the photolysis values.

The observed value of $P(NO_z)$, 2.1 ± 0.4 pptv/s, is a lower limit to the true value of $L(RO_x)$ since non-NO_x related RO_x losses (R14-R17) do not form NO_z. We estimate that

the water-assisted self reaction of HO_2 accounts for approximately 0.1 pptv/s, based on an estimated HO_2 mixing ratio of 40 pptv and the measured water vapor concentration. The estimated rate of the reaction between RO_2 and HO_2 using 40 pptv for both species and a rate constant of 10^{-11} molecules cm^{-3} s^{-1} (Atkinson, 1994) is 0.3 pptv/s, though there are strong indications that this rate constant is high by up to an order of magnitude (Lelieveld et al., 2008; Thornton et al., 2002). Heterogeneous loss of HO_2 is possibly the most uncertain RO_x loss process (Emmerson et al., 2007; Thornton et al., 2008).

The comparison of the calculated $P(RO_x)$ value (1.7 ± 0.5 pptv/s) and $L(RO_x)$ inferred from $P(NO_z)$ (2.1 ± 0.4 pptv/s) indicates both that the budget of RO_x sources and sinks is "closed" within the methodological uncertainties (i.e., $P(RO_x)$ has been shown to equal $L(RO_x)$) and that ozone production is indeed VOC-limited since $P(NO_z)$ is roughly equal to $L(RO_x)$. That ozone production is VOC-limited is in agreement with predictions from previous photochemical models (Lei et al., 2007; Tie et al., 2007) and recent measurements (Nunnermacker et al., 2008; Stephens et al., 2008). Although the large uncertainty bars preclude a more quantitative insight into RO_x sources, we note that it is not possible for $P(NO_z)$ to actually exceed $P(RO_x)$, assuming net formation of N_2O_5, NO_3, and HONO was a negligible portion of $P(NO_z)$. Either $P(NO_z)$ has been overestimated or $P(RO_x)$ has been underestimated. The latter possibility is likely, since the calculation of $P(RO_x)$ does not include the net source of RO_x from the photolysis of HONO, H_2O_2, or oxygenated VOCs beyond formaldehyde, acetaldehyde, and acetone. The HONO mixing ratio would have to exceed the calculated photostationary state HONO mixing ratio of $\sim$10 pptv by a factor of 10 to account for a net RO_x source of 0.3 pptv/s. We estimate that photolysis of glyoxal (CHOCHO) contributes at most an additional 0.1 pptv/s, based on the maximum glyoxal concentrations ($\sim$1 ppbv) observed previously in Mexico City (Volkamer et al., 2005). Studies of RO_x production that have utilized the Master Chemical Mechanism (Saunders et al., 2003) have invoked a large source of RO_x from oxygenated VOCs besides the three considered in our calculation of $P(RO_x)$ (Emmerson et al., 2007; Volkamer et al., 2007). It is not unreasonable that some combination of these sources could account for an additional 0.2–0.3 pptv/s. It is unlikely that the reaction of electronically excited NO_2 with water vapor acts as a significant RO_x source during the afternoon due to the small solar zenith angles (Li et al., 2008).

This use of NO_z measurements as a tool for gleaning information on RO_x loss rates may be useful in smog chamber experiments as well as stagnant air masses. The alternative, more common method of quantifying RO_x losses relies on the explicit calculation of the rate of each RO_x loss reaction, which requires accurate knowledge of the reactants OH, HO_2, and speciated RO_2 mixing ratios as well as the relevant rate constants, which are highly uncertain for many RO_2 reactions. We note that this analysis of the calculated RO_x production rate and the inferred RO_x loss rate does not provide information on the *interconversions* between OH, HO_2, and RO_2; actual measurements of those species would be required for that analysis.

In general, $P(O_x)$ increases with increasing RO_x production rates (Kleinman, 2005). The inferred value of $P(O_x)$ of 49 ppbv/h (13 pptv/s) for the observed $P(RO_x)$ rate of 1.7 ± 0.5 pptv/s also agrees well with that predicted by Lei et al. (2007). This agreement is perhaps fortuitous given the uncertainties of both methods.

$P(RO_x)$ exhibits an interesting asymmetry over the course of the day. Due to the elevated concentrations of oxygenated VOCs in the morning, $P(RO_x)$ (excluding alkene ozonolysis) peaks at a value of 1.6 pptv/s at 11:00, whereas peak actinic flux and photolysis frequencies peak more than an hour later. This overall temporal profile was observed during several but not all days at PTP. The peak and mean daytime values of $P(RO_x)$ on 12 March were higher than on any other day at PTP between 8 March and 18 March. The mean value of $P(RO_x)$ between 9:00 and 16:00 during this span of 11 days, under various meteorological conditions, was 0.6 pptv/s, whereas on 12 March it was 1.2 pptv/s.

Another interesting feature of RO_x production on 12 March is that despite extremely high O_3 mixing ratios ($>$150 ppbv), O_3 photolysis accounted for at most 43% of $P(RO_x)$ excluding alkene ozonolysis, similar to observations in the city center in 2003 (Volkamer et al., 2007). The relative humidity was low on 12 March (less than 17% after noon), limiting the rate of reaction between water vapor and $O(^1D)$ produced from the photolysis of ozone. The relative importance of O_3 photolysis as a RO_x source increased later in the month when the relative humidity increased greatly. The oxygenated VOCs (primarily HCHO) that account for the largest fraction of $P(RO_x)$ are both emitted directly in Mexico City at rates higher than in the US and are produced by VOC oxidation (Garcia et al., 2006; Kolb et al., 2004; Zavala et al., 2006).

3.5 Efficiency of ozone production

The efficiency of ozone production can be quantified with regard either to the NO_x catalytic cycle or to the oxidation of VOCs. The number of ozone molecules that are produced per molecule of NO_x before the NO_x is removed from active photochemistry is known as the ozone production efficiency (OPE) of NO_x. Similarly, the amount of ozone that can be produced by the oxidation of individual VOCs has been studied in laboratory studies, yielding quantities such as the ozone creation potential (Derwent et al., 1996) and the maximum incremental reactivity (Carter et al., 1995). We examine ozone production in Mexico City using both the NO_x-based OPE metric and a new VOC-based metric that uses the correlation of the $\Delta[O_x]/\Delta[CO]$ ratio with an aromatic-VOC based photochemical clock.

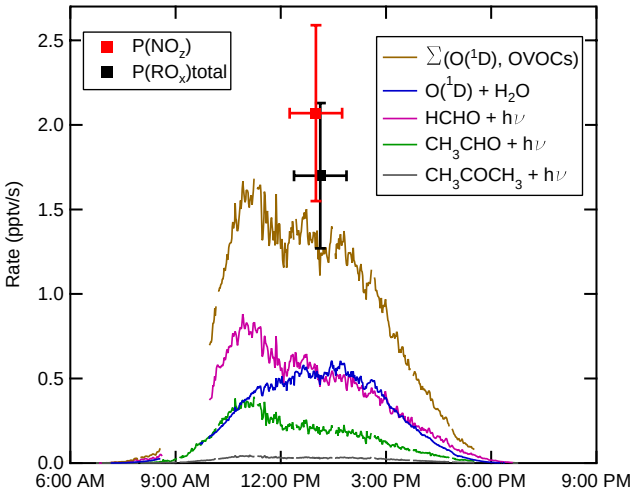

Fig. 5. Comparison of the NO_z production rate with the RO_x production rate during the afternoon of 12 March. RO_x production rates from the photolysis of O_3, HCHO, CH_3CHO, and acetone are depicted as lines, with the sum depicted by the brown line (OVOC = oxygenated volatile organic compound). The total $P(RO_x)$ value (black square) is calculated as the sum of the photolytic RO_x sources and an estimated 0.4 pptv/s from alkene ozonolysis. The red square demarks the average NO_z production rate observed between 12:15 and 13:15.

PTP is an excellent site for examining both of these approaches given the known meteorology, the lack of proximate emission sources, and (for one hour during the afternoon of 12 March 2006) the quantified production and loss rates of both O_x and NO_z.

3.5.1 Ozone production efficiency of NO_x

The OPE of NO_x has been extensively discussed over the last 20 years (Lin et al., 1988; Nunnermacker et al., 2000; Wang et al., 1998). The instantaneous OPE is usually defined as $P(O_x)/P(NO_z)$, whereas the integrated OPE for an observed air mass is usually inferred by the correlation between O_x and NO_z (i.e., $\Delta[O_x]/\Delta[NO_z]$). The instantaneous OPE of an air mass is expected to vary with time, and is affected by the temporal evolution of the partitioning of RO_x among OH, HO_2, and RO_2 and the partitioning of NO_x between NO and NO_2.

Inferred and/or modeled OPE values range from 2–8 in urban (high-NO_x) settings and power plant plumes (Kleinman, 2000;Nunnermacker et al., 2000) up to 46 for the mean OPE of the southern hemisphere (Wang et al., 1998). The large range of values reflects the non-linear dependence of ozone production on its chemical precursors. In general, the OPE increases with the VOC reactivity to NO_x ratio and is highest in chemical environments in which ozone production is NO_x-limited. The interpretation of inferred OPE values using observations of $\Delta[O_x]/\Delta[NO_z]$ is complicated by photochemical and depositional losses of NO_z (Nunnermacker et al., 1998) and O_x. The OPE can also be difficult to interpret if the observed air masses are inhomogeneous – i.e., if the observed ozone is the result of multiple air masses of different histories that have mixed prior to the observations (Liang and Jacobson, 2000).

The role that thermally labile peroxyacyl nitrates (such as PAN) have as a reservoir of both RO_x and NO_x complicates the interpretation of the OPE. Net formation of peroxyacyl nitrates acts as a temporary sink of NO_x (and O_x). Subsequent thermal decomposition of peroxyacyl nitrates releases the NO_x, allowing it to catalyze the production of more O_3 - quite possibly in chemical environments where $OPE_{(Inst)}$ is different than where the NO_x was initially emitted. Thus the number of ozone molecules produced from each NO_x depends on what temporal and spatial scale is considered. Shon et al. (2008) and Nunnermacker et al. (2008) report OPE values (inferred from $\Delta[O_x]/\Delta[NO_z]$) that range from 5 within the boundary layer up to 8.5 in the marine free troposphere outside of Mexico City. The timing of NO_x emissions can also affect OPE values, since at night NO_x emissions can lead to net destruction of O_x through reactions involving NO_3 and N_2O_5 (Brown et al., 2006). The OPE values determined below in Sect. 3.5.2 and 3.5.3 are focused on daytime chemistry on a time scale of less than 10 h.

Between 12:15 and 13:15 on 12 March 2006, the value of $P(O_x)/P(NO_z)$ using the values for $P(O_x)$ and $P(NO_z)$ derived in Sect. 3.1 and 3.2 was 6.4. This value for the OPE reflects the *gross* O_x produced per NO_x. This value is greater than the correlation between the O_x and NO_z concentrations during this hour (5.4), which is more a measure of the *net* O_x produced per NO_x, and is also affected by deposition of NO_z. The correlation is higher when all data between 09:00 and 16:00 on both 12 March and 11 March are included. These two days experienced similar air masses and a comparable range of photochemical ages (as determined by $[NO_z]/[NO_y]$). The slope of the graph of O_x versus NO_z (Fig. 5) for these two days is 6.2±0.2. To infer the gross O_x produced per NO_x, the slope can be "corrected" to account for losses of O_x. Additionally, the NO_z measurements can be corrected to account for cumulative NO_z losses (deposition). As discussed in Sect. 3.3.1, we can infer that between 12:15 and 13:15 on 12 March approximately 9% of the NO_z was removed from the system by a comparison of the $\Delta[NO_y]/\Delta[CO]$ ratio with that expected based on the cumulative emissions of NO_x and CO. If the emission ratio of NO_x/CO were actually a constant value of 0.05 throughout the day, the "corrected" value of $[NO_z]$ (i.e., the value of $[NO_z]$ that would have been measured had there been no NO_z deposition) can be expressed by Eq. (4):

$$[NO_{z(CORRECTED)}] = 0.05 \times ([CO] - 130) - [NO_x] \quad (5)$$

where the NO_y measurements are ignored and instead are simulated by the CO measurements and scaled by the NO_x/CO emission ratio.

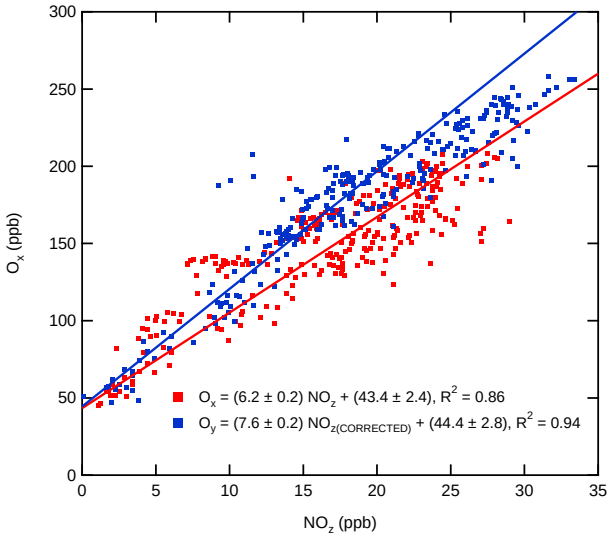

Fig. 6. Inference of the short-term ozone production efficiency (OPE) at PTP on 11 and 12 March 2006 between 08:30 and 18:00. The red points use the raw O_x and NO_z data. Correcting for losses of both species produces the blue points (see text).

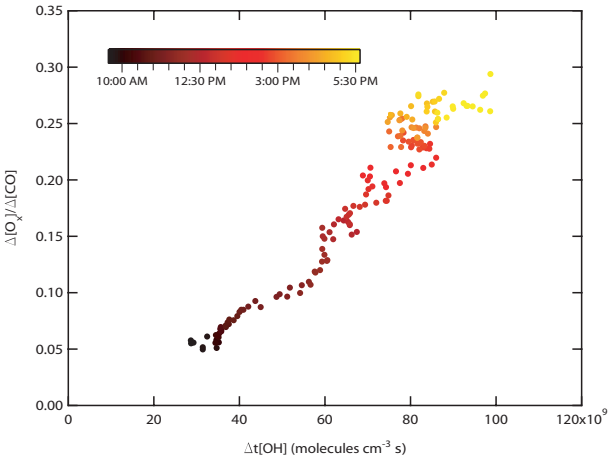

Fig. 7. Correlation of $\Delta[O_x]/\Delta[CO]$ on 12 March 2006 with cumulative OH exposure ($\Delta t[OH]$) as inferred by a C9-aromatic photochemical clock.

The total O_x lost is determined by the integrated O_x destruction mechanisms described in Sect. 3.2. We use the quantity "O_y" to represent the total integrated O_x production. In Sect. 3.2 the quantity $0.8\times P(NO_z)$ was used to estimate total O_x loss rate via NO_2 oxidation, which accounted for approximately 50% of the total O_x loss between 12:15 and 13:15. If this value (50%) does not vary greatly over the course of the day, then total integrated O_x losses can be approximated by Eq. (5):

$$[O_Y] = [O_x] + 1.6[NO_z] \quad (6)$$

The true percentage undoubtedly varies over the course of the day, contributing to the uncertainty of this approximation. $[O_y]$ is between 5% and 25% higher than $[O_x]$.

Figure 6 depicts the correlations on 11 and 12 March 2006 between O_x and NO_z, which has a slope of 6.2, and that between O_y and $NO_{z(CORRECTED)}$, which has a higher slope of 7.6. In most other cases where inferred OPE values have been corrected for losses (Nunnermacker et al., 1998), the corrected OPE have been lower than the uncorrected OPE, in contrast to the case here. This is because the correction for O_x losses is greater than the correction for NO_z. This is partially just a difference in approach: by using O_y instead of O_x, the approach used here reflects the integrated ozone production rather than the *net* ozone production per molecule of NO_x oxidized. In the air masses examined, NO_y was mostly conserved; the maximum correction to NO_z was 20%. For more highly aged air masses, the relative magnitude of the O_x and NO_z corrections might be different. The oxidation of NO_2 was the dominant loss of O_x in the young air masses observed, which had undergone less than 10 h of atmospheric oxidation. The contribution of this O_x loss process likely decreased in importance after the NO_x/NO_y decreased to lower values ($\sim$0.1).

The similarity between the corrected slope and the uncorrected slope indicate that the OPE can be reasonably approximated during one day of photochemistry in Mexico City by the correlation of $[O_x]$ with $[NO_z]$. Slightly higher O_x/NO_z correlations were observed elsewhere in the city – for example, our measurements at Santa Ana during an ozone-south meteorological episode (deFoy et al., 2006) on 24 March 2006 yielded an (uncorrected) OPE value of 7.5±0.3. The values derived here (6–8) are within the range of 4 to 12 calculated by Lei et al. (Lei et al., 2007) for NO_x mixing ratios greater than 10 ppbv.

3.5.2 $\Delta[O_x]/\Delta[CO]$ and a VOC-based photochemical clock

Since CO is a relatively unreactive tracer of dilution, the quantity $\Delta[O_x]/\Delta[CO]$ can be interpreted as the dilution-adjusted measure of integrated ozone production, similar to the use of the ratio of organic aerosol to CO in studies of secondary organic aerosol formation (Kleinman et al., 2008). In the MCMA, on-road vehicles are the largest source of CO by far, accounting for over 99% of total CO emissions (CAM, 2008). VOCs are emitted by on-road vehicles (34% by mass) as well as area sources (46%) and industrial sources (17%), though the most reactive VOCs are emitted by on-road vehicles (CAM, 2008; Velasco et al., 2007). Thus CO and the most important ozone-producing VOCs are co-emitted, and emissions of total VOCs and CO overlap spatially. The CO mixing ratio is in most cases proportional to the total emissions of VOCs, though the proportionality constant (e.g., the VOC/CO emission ratio) depends greatly on the nature of the emission sources .

The increase in $\Delta[O_x]/\Delta[CO]$ can be related to the cumulative OH exposure $\Delta t[OH]$ (photochemical age) of the observed air mass using a C9-aromatic photochemical clock (Herndon et al., 2008; Roberts et al., 1984). The photochemical age we use is based on PTR-MS measurements of benzene and the sum of C9-aromatic compounds, which include C_9H_{12} and C_8H_8O isomers. The calculation is described in Herndon et al. (2008). Since the air masses observed consisted of a combination of fresh emissions and aged emissions and are best described by a distribution of photochemical ages, the single values derived using this photochemical clock are meant only as an estimate of the average OH exposure of the air.

Figure 7 depicts the correlation between $\Delta[O_x]/\Delta[CO]$ and $\Delta t[OH]$ between 09:00 and 17:00 on 12 March 2006, with $\Delta[O_x]/\Delta[CO]$ calculated as ($[O_x]$–45)/([CO]–130). Background values of 45 ppbv for O_x and 130 ppbv for CO are based on observations at night, when PTP was well above the nocturnal boundary layer. As expected, $\Delta[O_x]/\Delta[CO]$ increases with $\Delta t[OH]$, and there is little scatter in the plot (R^2>0.9). The slope of a linear fit (not shown) is 3.8×10^{-12} ppbv O_x ppbv^{-1} CO (molecules OH cm^{-3} s)$^{-1}$, though it appears that it may be higher for the afternoon than for the morning data. This is supported by the fact that $\Delta[O_x]/\Delta[CO]$ should equal zero when $\Delta t[OH]$ is zero. Observations on other days were similar, with most slopes within the range of 3.6×10^{-12} to 5.6×10^{-12} ppbv O_x ppbv^{-1} CO (molecules OH cm^{-3} s)$^{-1}$. The correlation was poor when the air masses observed were affected by a range of emission sources within the same day (e.g., biomass burning vs. urban emissions).

Variation in the slopes by time of day could be related to differences in ozone photochemistry between the morning and afternoon. Within the boundary layer, overall concentrations of NO_x and VOCs are highest in the morning because of the shallow mixing depth (typically less than 500 m between 06:00 and 11:00). Additionally, the VOC mixture differs: it consists primarily of unoxidized, primary VOCs in the morning and a mix of primary and secondary VOCs (e.g., oxygenated VOCs) in the afternoon. Thus it is conceivable that for a given amount of OH exposure, the different photochemical conditions could lead to differences in the slope of $\Delta[O_x]/\Delta[CO]$ vs. $\Delta t[OH]$ (e.g., if secondary VOCs are more efficient at producing ozone). Changes in the slope of Fig. 7 could also simply be caused by perturbations to the $\Delta[O_x]/\Delta[CO]$ ratio and the inferred OH exposure ($\Delta t[OH]$) due to changes in the emission ratios of the aromatic VOCs and CO.

A plot of $\Delta[O_x]/\Delta[NO_y]$ vs. $\Delta t[OH]$ (not shown) looks similar to Fig. 7 since NO_y was mostly conserved in the air masses observed. The quantity $\Delta[O_x]/\Delta[NO_y]$ is related to the OPE of NO_x in that it expresses the average number of ozone molecules that have been produced per molecule of NO_x emitted (rather than ozone produced per NO_x oxidized). This quantity is initially zero in fresh emissions that have not undergone photochemical conversion, when $[NO_x]$ and $[NO_y]$ are equal. As the air mass is photochemically processed, O_x is produced, NO_x is converted into NO_z, and there are fresh emissions of NO_x. Ignoring the effects of O_x and NO_y loss/deposition, the value of $\Delta[O_x]/\Delta[NO_y]$ should approach the integrated OPE value of $\Delta[O_x]/\Delta[NO_z]$, since NO_y consists primarily (>90%) of NO_z in highly aged air. On 12 March 2006, the value of $\Delta[O_x]/\Delta[NO_y]$ steadily increased during the day and reached 7 by 17:00, which is comparable to the OPE inferred in Fig. 6. This is expected since $[NO_z]$ and $[NO_y]$ are close in magnitude then, and thus $\Delta[O_x]/\Delta[NO_y]\approx\Delta[O_x]/\Delta[NO_z]$.

Comparison of the correlation of $\Delta[O_x]/\Delta[CO]$ with $\Delta t[OH]$ observed in Mexico City to other locations should be done with the caveat that the values are greatly affected by the VOC/CO emission ratios. This metric may be most useful for comparing ozone production during different times of day or under different meteorological conditions at locations when the VOC/CO ratio does not vary greatly.

4 Conclusions

Measurements of several ambient gas-phase and particulate species from a unique mountain-top site in Mexico City have been used to characterize the chemistry of ozone production, nitrogen oxides, and the RO_x budget, with an emphasis on one hour of data during which the rise of the mixing depth was slow. Overall, the observations agree well with the predictions of photochemical models (Lei et al., 2007; Tie et al., 2007).

The observed time rate of change in the mixing ratios of O_x and NO_z combined with calculations of the O_x loss rates during the case study period (12 March 2006) were used to infer an O_x production rate of 49 ppbv/h and an NO_z production rate of 7.6 ppbv/h. The dominant loss process for O_x was the oxidation of NO_2 to NO_z compounds (e.g., HNO_3); photolysis of O_3 was a minor contributor to O_x loss due to the low relative humidity. A decrease in $([HNO_{3(g)}]+[NO^-_{3(PM1)}])/[NO_z]$ with increasing $[NO_z]/[NO_y]$ was observed. Deposition of HNO_3 was a minor contributor to this trend, whereas a shift of the aerosol nitrate size distribution from the accumulation mode to the coarse mode and possibly a decrease in the HNO_3 production rate relative to total NO_z production are plausible explanations. A comparison of RO_x production rates and the observed increase in NO_z during a period of stagnant air indicates that O_x production was VOC-limited and that the RO_x budget was closed (i.e., $P(RO_x)=L(RO_x)$) to within the methodological uncertainties.

The ozone production efficiency of NO_x on a time scale of one day was approximately 7 as inferred by the correlation of $[O_x]$ to $[NO_z]$. Corrections to this correlation that account for losses of O_x and NO_z increase the inferred value of the ozone production efficiency by less than 30%. A new metric for assessing the efficiency of ozone production has been

proposed and is based on the correlation of the $[O_x]$:[CO] ratio with the average OH exposure as inferred by ratios of aromatic VOCs.

Although this analysis focused on only a short time period, the chemistry characterized is in agreement with previous modeling work and lends confidence to the state of knowledge regarding ozone chemistry, nitrogen oxides, and the underlying fast radical chemistry. A few aspects of the chemistry, however, have not been commonly observed in other locations. For example, gas-phase HNO_3 comprised a small fraction of NO_z (less than 15% usually), whereas particulate nitrate comprised a much larger fraction - mainly due to the high concentrations of NH_3. The photolysis of ozone and subsequent reaction of $O(^1D)$ with water vapor was a minor destruction channel for O_3 during the first $\sim$24 h of atmospheric chemistry, and even during high O_3 events ($[O_3]>150$ ppbv) ozone photolysis accounted for less than half of total RO_x sources in dry air masses. Although rare in the literature, these characteristics are not necessarily unique considering that the atmosphere above most developing megacities remains largely uncharacterized.

Acknowledgements. This work was funded in part by NSF grants (ATM-528227 & ATM-0528170) and DOE grants (DE-FGO2-05ER63982 & DE-FGO2-05ER63980). We gratefully acknowledge Luisa Molina and Linsey Marr for providing the two chemiluminescence analyzers. We thank Manuel Quiñones of Televisa for providing power and on-site support at PTP, Rafael Ramos for logistical assistance, Sasha Madronich of NCAR for assistance with the TUV model, and Delphine Farmer for helpful conversations. The United States Environmental Protection Agency through its Office of Research and Development collaborated in the research described here. It has been subjected to Agency review and approved for publication.

Edited by: S. Madronich

References

Atkinson, R.: Gas-phase tropospheric chemistry of organic compounds, Journal of Physical Chemistry Ref. Data, M2, 1994.

Brown, S. S., Neuman, J. A., Ryerson, T. B., Trainer, M., Dubé, W. P., Holloway, J. S., Warneke, C., De Gouw, J. A., Donnelly, S. G., and Atlas, E.: Nocturnal odd-oxygen budget and its implications for ozone loss in the lower troposphere, Geophys. Res. Lett., 33, doi:10.1029/2006GL025900, 2006.

Calvert, J. G., Atkinson, R., Kerr, J. A., Madronich, S., Moortgat, G. K., Wallington, T. J., and Yarwood, G.: The Mechanisms of Atmospheric Oxidation of the Alkenes, Oxford University Press, Oxford, 277–278, 2000.

CAM: Inventario de emisiones 2006 de la Zona Metropolitana del Valle de Mexico, http://www.sma.df.gob.mx, 2008.

Canagaratna, M. R., Jayne, J. T., Jimenez, J. L., Allan, J. D., Alfarra, M. R., Zhang, Q., Onasch, T. B., Drewnick, F., Coe, H., Middlebrook, A., Delia, A., Williams, L. R., Trimborn, A. M., Northway, M. J., DeCarlo, P. F., Kolb, C. E., Davidovits, P., and Worsnop, D. R.: Chemical and microphysical characaterization of ambient aerosols with the Aerodyne Aerosol Mass Spectrometer, Mass Spectrom. Rev., 26, 185–222, doi:10.1002/mas.20115, 2007.

Cantrell, C., Anderson, R., Mauldin, L., Kociuch, E., McCoy, J., Eisele, F., Apel, E., Reimer, D., Hills, A., Karl, T., Knapp, D., Montzka, D., Fried, A., Weibring, P., Walega, W., Richter, D., Flocke, F., Zheng, W., Emmons, L., Crawford, J., Dunlea, E., DeCarlo, P., Clarke, T., Howell, S., Cohen, R., Shetter, R., Hall, S., Russell, L., Kok, G., Weber, R., Madronich, S., Wennberg, P., Crounse, J., McCabe, D., and Holloway, J.: HO_x Behavor as Observed Aboard the C-130 during MILAGRO, MILAGRO Science Meeting, Mexico City, 2007.

Carslaw, N., Creasey, D. J., Harrison, D., Heard, D. E., Hunter, M. C., Jacobs, P. J., Jenkin, M. E., Lee, J. D., Lewis, A. C., Pilling, M. J., Saunders, S. M., and Seakins, P. W.: OH and HO2 radical chemistry in a forested region of north-western Greece, Atmos. Environ., 35, 4725–4737, 2001.

Carter, W. P. L., Pierce, J. A., Luo, D., and Malkina, I. L.: Environmental chamber study of maximum incremental reactivities of volatile organic compounds, Atmos. Environ., 29, 2499–2511, 1995.

Daum, P. H., Kleinman, L. I., Imre, D., Nunnermacker, L. J., Lee, Y. N., Springston, S. R., Newman, L., Weinstein-Lloyd, J., Valente, R. J., Imhoff, R. E., Tanner, R. L., and Meagher, J. F.: Analysis of O_3 formation during a stagnation episode in central Tennessee in summer 1995, J. Geophys. Res.-Atmos., 105, 9107–9119, 2000.

de Foy, B., Caetano, E., Magaña, V., Zitácuaro, A., Cárdenas, B., Retama, A., Ramos, R., Molina, L. T., and Molina, M. J.: Mexico City basin wind circulation during the MCMA-2003 field campaign, Atmos. Chem. Phys., 5, 2267–2288, 2005, http://www.atmos-chem-phys.net/5/2267/2005/.

de Foy, B., Varela, J. R., Molina, L. T., and Molina, M. J.: Rapid ventilation of the Mexico City basin and regional fate of the urban plume, Atmos. Chem. Phys., 6, 2321–2335, 2006, http://www.atmos-chem-phys.net/6/2321/2006/.

de Foy, B., Fast, J. D., Paech, S. J., Phillips, D., Walters, J. T., Coulter, R. L., Martin, T. J., Pekour, M. S., Shaw, W. J., Kastendeuch, P. P., Marley, N. A., Retama, A., and Molina, L. T.: Basin-scale wind transport during the MILAGRO field campaign and comparison to climatology using cluster analysis, Atmos. Chem. Phys., 8, 1209–1224, 2008, http://www.atmos-chem-phys.net/8/1209/2008/.

de Gouw, J. A., Middlebrook, A. M., Warneke, C., Goldan, P. D., Kuster, W. C., Roberts, J. M., Fehsenfeld, F. C., Worsnop, D. R., Canagaratna, M. R., Pszenny, A. A. P., Keene, W. C., Marchewka, M., Bertman, S. B., and Bates, T. S.: Budget of organic carbon in a polluted atmosphere: Results from the New England Air Quality Study in 2002, J. Geophys. Res.-Atmos., 110, doi:10.1029/2004JD005623, 2005.

de Gouw, J. A., Warneke, C., Stohl, A., Wollny, A. G., Brock, C. A., Cooper, O. R., Holloway, J. S., Trainer, M., Fehsenfeld, F. C., Atlas, E. L., Donnelly, S. G., Stroud, V., and Lueb, A.: Volatile organic compound composition of merged and aged forest fires from Alaska and Western Canada, J. Geophys. Res., 111, doi:10.1029/2005JD006175, 2006.

deFoy, B., Varela, J. R., Molina, L. T., and Molina, M. J.: Rapid ventilation of the Mexico City basin and regional fate of the urban plume, Atmos. Chem. Phys., 6, 2321–2335, 2006, http://www.atmos-chem-phys.net/6/2321/2006/.

Derwent, R. G., Jenkin, M. E., and Saunders, S. M.: Photochemical ozone creation potentials for a large number of reactive hydrocarbons under European conditions, Atmos. Environ., 30, 181–199, 1996.

Drewnick, F., Hings, S. S., DeCarlo, P., Jayne, J. T., Gonin, M., Fuhrer, K., Weimer, S., Jimenez, J. L., Demerjian, K. L., Borrman, S., and Worsnop, D. R.: A New Time-of-Flight Aerosol Mass Spectrometer (TOF-AMS) – Instrument Description and First Field Deployment, Aerosol Sci. Technol., 39, 637–658, 2005.

Dusanter, S., Vimal, D., Stevens, P. S., Volkamer, R., and Molina, L. T.: Measurements of OH and HO_2 concentrations during the MCMA-2006 field campaign Part 1: Deployment of the Indiana University laser-induced fluorescence instrument, Atmos. Chem. Phys., 9, 1665–1685, 2009, http://www.atmos-chem-phys.net/9/1665/2009/.

Emmerson, K. M., Carslaw, N., Carslaw, D. C., Lee, J. D., McFiggans, G., Bloss, W. J., Gravestock, T., Heard, D. E., Hopkins, J., Ingham, T., Pilling, M. J., Smith, S. C., Jacob, M., and Monks, P. S.: Free radical modelling studies during the UK TORCH Campaign in Summer 2003, Atmos. Chem. Phys., 7, 167–181, 2007, http://www.atmos-chem-phys.net/7/167/2007/.

Farmer, D. K., Cohen, R. C., Perring, A. E., et al.: NO_y partitioning and the role of alkyl nitrates in air quality in the Mexico City area, Atmos. Chem. Phys., in preparation, 2009.

Fast, J. D., De Foy, B., Acevedo Rosas, F., Caetano, E., Carmichael, G., Emmons, L., McKenna, D., Mena, M., Skamarock, W., Tie, X., Coulter, R. L., Barnard, J. C., Wiedinmyer, C., and Madronich, S.: A meteorological overview of the MILAGRO field campaigns, Atmos. Chem. Phys., 7, 2233–2257, 2007, http://www.atmos-chem-phys.net/7/2233/2007/.

Fountoukis, C., Nenes, A., Sullivan, A., Weber, R., VanReken, T., Fischer, M., Matias, E., Moya, M., Farmer, D., and Cohen, R. C.: Thermodynamic characterization of Mexico City aerosol during MILAGRO 2006, Atmos. Chem. Phys., 9, 2141–2156, 2009, http://www.atmos-chem-phys.net/9/2141/2009/.

Garcia, A. R., Volkamer, R., Molina, L. T., Molina, M. J., Samuelson, J., Mellqvist, J., Galle, B., Herndon, S. C., and Kolb, C. E.: Separation of emitted and photochemical formaldehyde in Mexico City using a statistical analysis and a new pair of gas-phase tracers, Atmos. Chem. Phys., 6, 4545–4557, 2006, http://www.atmos-chem-phys.net/6/4545/2006/.

Geyer, A., Alicke, B., Ackermann, R., Martinez, M., Harder, H., Brune, W., Di Carlo, P., Williams, E., Jobson, T., Hall, S., Shetter, R., and Stutz, J.: Direct observations of daytime NO_3: Implications for urban boundary layer chemistry, J. Geophys. Res., 108, 4368, doi:4310.1029/2002JD002967, 2003.

Hennigan, C. J., Sullivan, A. P., Fountoukis, C. I., Nenes, A., Hecobian, A., Vargas, O., Peltier, R. E., Case Hanks, A. T., Huey, L. G., Lefer, B. L., Russell, A. G., and Weber, R. J.: On the volatility and production mechanims of newly formed nitrate and water soluble organic aerosol in Mexico City, Atmos. Chem. Phys., 8, 3761–3768, 2008, http://www.atmos-chem-phys.net/8/3761/2008/.

Herndon, S., Onasch, T., Wood, E. C., Kroll, J. H., Canagaratna, M., Jayne, J., Zavala, M., Knighton, W. B., Mazzoleni, C., Dubey, M. K., Ulbrich, I., Jimenez, J. L., Seila, R., de Gouw, J. A., De Foy, B., Fast, J., Molina, L., Kolb, C. E., and Worsnop, D. R.: The correlation of secondary organic aerosol with odd oxygen in Mexico City, Geophys. Res. Lett., 35, doi:10.1029/2008GL034058, 2008.

Herndon, S. C., Jayne, J. T., Zahniser, M. S., Worsnop, D. R., Knighton, B., Alwine, E., Lamb, B. K., Zavala, M., Nelson, D. D., and McManus, J. B.: Characterization of urban pollutant emission fluxes and ambient concentration distributions using a mobile laboratory with rapid response instrumentation, Faraday Discuss, 130, 327–339, 2005.

Herndon, S. C., M. S. Zahniser, D. D. Nelson Jr., J. Shorter, J. B. McManus, R. Jiménez, C. Warneke, and Gouw, J. A. d.: Airborne measurements of HCHO and HCOOH during the New England Air Quality Study 2004 using a pulsed quantum cascade laser spectrometer, J. Geophys. Res., 112, D10S03, doi:10.1029/2006JD007600., 2007.

Khan, H. A.: Benzene's toxicity: a consolidated short review of human and animal studies, Human Exp. Tox., 26, 677–685, 2007.

Kleinman, L. I.: Ozone process insights from field experiments – part II: Observation-based analysis for ozone production, Atmos. Environ., 34, 2023–2033, 2000.

Kleinman, L. I., Daum, P. H., Imre, D., Lee, Y. N., Nunnermacker, L. J., Springston, S. R., Weinstein-Lloyd, J., and Rudolph, J.: Ozone production rate and hydrocarbon reactivity in 5 urban areas: A cause of high ozone concentration in Houston, Geophys. Res. Lett., 29(10), 1467, doi:10.1029/2001GL014569, 2002.

Kleinman, L. I.: The dependence of tropospheric ozone production rate on ozone precursors, Atmos. Environ., 39, 575–586, 2005.

Kleinman, L. I., Springston, S. R., Daum, P. H., Lee, Y. N., Nunnermacker, L. J., Senum, G. I., Wang, J., Weinstein-Lloyd, J., Alexander, M. L., Hubbe, J., Ortega, J., CAnagaratna, M. R., and Jayne, J.: The time evolution of aerosol composition over the Mexico City plateau, Atmos. Chem. Phys., 8, 1559–1575, 2008, http://www.atmos-chem-phys.net/8/1559/2008/.

Knighton, W. B., Fortner, E. C., Herndon, S. C., Wood, E. C., Canagaratna, M., Jayne, J., Kroll, J. H., Onasch, T., Trimborn, A., Worsnop, D., and Kolb, C.: Examination of Biomass Burning Tracer Signatures in Urban Environments, EOS, Transactions, American Geophysical Union, A33D-1569, 2007.

Kolb, C. E., Herndon, S. C., McManus, J. B., Shorter, J. H., Zahniser, M. S., Nelson, D. D., Jayne, J. T., Canagaratna, M. R., and Worsnop, D. R.: Mobile Laboratory with Rapid Response Instruments for Real-Time Measurements of Urban and Regional Trace Gas and Particulate Distributions and Emission Source Characteristics, Environ. Sci. Technol., 38, 5694–5703, 2004.

Laskin, A., Wietsma, T. W., Krueger, B. J., and Grassian, V. H.: Heterogenous chemistry of individual mineral dust particles with nitric acid: A combined CCSEM/EDX, ESEM, and ICP-MS study, J. Geophys. Res.-Atmos., 110(D10), doi:10.1029/2004JD005206, 2005.

Lei, W., de Foy, B., Zavala, M., Volkamer, R., and Molina, L. T.: Characterizing ozone production in the Mexico City Metropolitan Area: a case study using a chemical transport model, Atmos. Chem. Phys., 7, 1347–1366, 2007, http://www.atmos-chem-phys.net/7/1347/2007/.

Lelieveld, J., Butler, T. M., Crowley, J. N., Dillon, T. J., Fischer, H., Ganzeveld, L., Harder, H., Lawrence, M. G., Martinez, M., Taraborrelli, D., and Williams, J.: Atmospheric oxidation capacity sustained by a tropical forest, Nature, 452, 737–740, 2008.

Li, S., Matthews, J., and Sinha, A.: Atmospheric Hydroxyl Radical Production from Electronically Excited NO_2 and H_2O, Science,

319, 1657–1660, 2008.

Liang, J. and Jacobson, M. Z.: Effects of subgrid segregation on ozone production efficiency in a chemical model, Atmos. Environ., 34, 2975–2982, 2000.

Lim, Y. B. and Ziemann, P. J.: Products and mechanism of secondary organic aerosol formation from reactions of n-alkanes with OH radicals in the presence of NO_x, Environ. Sci. Technol., 39, 9229–9236, 2005.

Lin, X., Trainer, M., and Liu, S. C.: On the Nonlinearity of the Tropospheric Ozone Production, J. Geophys. Res., 93, 15879–15888, 1988.

Lindinger, W., Hansel, A., and Jordan, A.: Proton-transfer-reaction mass spectrometry (PTR-MS): on-line monitoring of volatile organic compounds at pptv levels, Chemical Society Reviews, 27, 347, 1998.

Liu, P. S. K., Deng, R., Smith, K. A., Williams, L. R., Jayne, J. T., Canagaratna, M. R., Moore, K., Onasch, T. B., Worsnop, D. R., and Deshler, T.: Transmission Efficiency of an Aerodynamic Focusing Lens System: Comparison of Model Calculations and Laboratory Measurements for the Aerodyne Aerosol Mass Spectrometer, Aerosol Sci. Technol., 41, 721–733, 2007.

Madronich, S.: Chemical Evolution of gaseous air pollutants downwind of tropical megacities: Mexico City case study, Atmos. Environ., 40, 6012–6018, 2006.

Matthew, B. M., Middlebrook, A. M., and Onasch, T. B.: Collection Efficiencies in an Aerodyne Aerosol Mass Spectrometer as a Function of Particle Phase for Laboratory Generated Aerosols, Aerosol Sci. Technol., 42, 884–898, 2008.

McCreanor, J., Cullinan, P., Nieuwenhuijsen, M. J., Stewart-Evans, J., Malliarou, E., Jarup, L., Harrington, R., Svartengren, M., Han, I., Ohman-Strickland, P., Chung, K. F., and Zhang, J.: Respiratory Effects of Exposure to Diesel Traffic in Persons with Asthma, The New England Journal of Medicine, 357, 2348-2358, 2007.

Moffet, R. C., de Foy, B., Molina, L. T., Molina, M. J., and Prather, K. A.: Measurement of ambient aerosols in northern Mexico City by single particle mass spectrometry, Atmos. Chem. Phys., 8, 4499–4516, 2008, http://www.atmos-chem-phys.net/8/4499/2008/.

Molina, L. T., Molina, M. J., Slott, R. S., Kolb, C. E., Gbor, P. K., Meng, F., Singh, R. B., Galvez, O., Sloan, J. J., Anderson, W. P., Tang, X., Hu, M., Xie, S., Shao, M., Zhu, T., Zhang, Y. H., Gurjar, B. R., Artaxo, P. E., Oyola, P., Gramsch, E., Hidalgo, D., and Gertler, A. W.: Air Quality in Selected Megacities, J. Air Waste Manage. Assoc., 55, 1–73, 2004.

Nelson, D. D., McManus, B., Urbanski, S., Herndon, S., and Zahniser, M. S.: High precision measurements of atmospheric nitrous oxide and methane using thermoelectrically cooled mid-infrared quantum cascade lasers and detectors, Spectroc. Acta Pt. A-Molec. Biomolec. Spectrom., 60, 3325–3335, 2004.

Nunnermacker, L. J., Imre, D., Daum, P. H., Kleinman, L., Lee, Y. N., Springston, S. R., Newman, L., Weinstein-Lloyd, J., Luke, W. T., Banta, R., Alvarez, R., Senff, C., Sillman, S., Holdren, M., Keigley, G. W., and Zhou, X.: Characterization of the Nashville urban plume on July 3 and July 18, 1995, J. Geophys. Res., 103, 28129–28148, 1998.

Nunnermacker, L. J., Kleinman, L. I., Imre, D., Daum, P. H., Lee, Y. N., Lee, J. H., Springston, S. R., Newman, L., and Gillani, N.: NO_y lifetimes and O_3 production efficiencies in urban and power plant plumes: Analysis of field data, J. Geophys. Res.-Atmos., 105, 9165–9176, 2000.

Nunnermacker, L. J., Weinstein-Lloyd, J. B., Hillery, B., Giebel, B., Kleinman, L. I., Springston, S. R., Daum, P. H., Gaffney, J., Marley, N., and Huey, G.: Aircraft and ground-based measurements of hydroperoxides during the 2006 MILAGRO field campaign, Atmos. Chem. Phys., 8, 7619–7636, 2008, http://www.atmos-chem-phys.net/8/7619/2008/.

Querol, X., Pey, J., Minguillon, M. C., Perez, N., Alastuey, A., Viana, M., Moreno, T., Bernabe, R. M., Blanco, S., Cardenas, B., Vega, E., Sosa, G., Escalona, S., Ruiz, H., and Artinano, B.: PM speciation and sources in Mexico during the MILAGRO-2006 Campaign, Atmos. Chem. Phys., 8, 111–128, 2008, http://www.atmos-chem-phys.net/8/111/2008/.

Roberts, J. M., Fehsenfeld, F. C., Liu, S. C., Bollinger, M. J., Hahn, C., Albritton, D. L., and Sievers, R. E.: Measurements of aromatic hydrocarbon ratios and NO_x concentrations in the rural troposphere: Estimates of air mass photochemical age and NO_x removal rate, Atmos. Environ., 18, 2421–2432, 1984.

Rogers, T. M., Grimsrud, E. P., Herndon, S. C., Jayne, J. T., Kolb, C. E., Allwine, E., Westberg, H., Lamb, B. K., Zavala, M., Molina, L. T., Molina, M. J., and Knighton, W. B.: On-road measurements of volatile organic compounds in the Mexico City metropolitan area using proton transfer reaction mass spectrometry, Int. J. Mass Spectrom., 252, 26–37, 2006.

Ryerson, T. B., Trainer, M., Holloway, J. S., Parrish, D. D., Huey, L. G., Sueper, D. T., Frost, G. J., Donnelly, S. G., Schauffler, S., Atlas, E. L., Kuster, W. C., Goldan, P. D., Hubler, G., Meagher, J. F., and Fehsenfeld, F. C.: Observations of ozone formation in power plant plumes and implications for ozone control strategies, Science, 292, 719–723, 2001.

Salcedo, D., Onasch, T. B., Dzepina, K., Canagaratna, M. R., Zhang, Q., Huffman, J. A., DeCarlo, P. F., Jayne, J. T., Mortimer, P., Worsnop, D. R., Kolb, C. E., Johnson, K. S., Zuberi, B., Marr, L. C., Volkamer, R. M., Molina, L. T., Molina, M. J., Cardenas, B., Bernabe, R. M., Marquez, C., Gaffney, J. S., Marley, N. A., Laskin, A., Shutthanandan, V., Xie, Y., Brune, W., Lesher, R., Shirley, T., and Jimenez, J. L.: Characterization of ambient aerosols in Mexico City during the MCMA-2003 campaign with aerosol mass spectrometry: results from the CENICA Supersite., Atmos. Chem. Phys., 6, 925–946, www.atmos-chem-phys.net/6/925/2006/, 2006.

San Martini, F. M., Dunlea, E. J., Grutter, M., Onasch, T. B., Jayne, J. T., Canagaratna, M. R., Worsnop, D. R., Kolb, C. E., Shorter, J. H., Herndon, S. C., Zahniser, M. S., Ortega, J. M., McRae, G. J., Molina, L. T., and Molina, M. J.: Implementation of a Markov Chain Monte Carlo method to inorganic aerosol modeling of observations from the MCMA-2003 campaign - Part I: Model description and application to the La Merced site, Atmos. Chem. Phys, 6, 4867–4888, 2006.

Sander, S. P., Friedl, R. R., Golden, D. M., Kurylo, M. J., Moortgat, G. K., Wine, P. H., Ravishankara, A. R., Kolb, C. E., Molina, M. J., Finlayson-Pitts, B. J., Huie, R. E., and Orkin, V. L.: Chemical Kinetics and Photochemical Data for Use in Atmospheric Studies: Evaluation Number 15, Jet Propulsion LaboratoryJPL Publication 06-2, 2006.

Saunders, S. M., Jenkin, M. E., Derwent, R. G., and Pilling, M. J.: Protocol for the development of the Master Chemical Mechanism, MCM v3 (Part A): tropospheric degradation of non-

aromatic volatile organic compounds, Atmos. Chem. Phys., 3, 161–180, 2003, http://www.atmos-chem-phys.net/3/161/2003/.

Seila, R. L., Main, H. H., Arriaga, J. L., Martinez, G., and Ramadan, A. B.: Atmospheric volatile organic compound measurements during the 1996 Paso del Norte Study, The Science of the Total Environment, 276, 153–169, 2001.

Shaw, W. J., Pekour, M. S., Coulter, R. L., Martin, T. J., and Walters, J. T.: The daytime mixing layer observed by radiosonde, profiler and lidar during MILAGRO, Atmos. Chem. Phys. Discuss., 15025–15065, 2007.

Shirley, T. R., Brune, W. H., Ren, X., Mao, J., Lesher, R., Cardenas, B., Volkamer, R., Molina, L. T., Molina, M. J., Lamb, B., Velasco, E., Jobson, T., and Alexander, M.: Atmospheric oxidation in the Mexico City Metropolitan Area (MCMA) during April 2003, Atmos. Chem. Phys., 6, 2753-2765, 2006, http://www.atmos-chem-phys.net/6/2753/2006/.

Shon, Z. H., Madronich, S., Song, S. K., Flocke, F. M., Knapp, D. J., Anderson, R. S., Shetter, R. E., Cantrell, C. A., Hall, S. R., and Tie, X.: Characteristics of the NO-NO_2-O_3 system in different chemical regimes during the MIRAGE-Mex field campaign, Atmos. Chem. Phys., 8, 7153–7164, 2008, http://www.atmos-chem-phys.net/8/7153/2008/.

Shorter, J. H., Herndon, S., Zahniser, M. S., Nelson, D. D., Wormhoudt, J., Demerjian, K. L., and Kolb, C. E.: Real-time Measurements of Nitrogen Oxide Emissions from In-use New York City Transit Buses using a Chase Vehicle, Environ. Sci. Technol, 39, 7991–8000, 2005.

Stephens, S., Madronich, S., Wu, F., Olson, J. B., Ramos, R., Retama, A., and Munoz, R.: Weekly patterns of Mexico City's surface concentrations of CO, NO_x, PM_{10} and O_3 during 1986–2007, Atmos. Chem. Phys., 8, 5313–5325, 2008, http://www.atmos-chem-phys.net/8/5313/2008/.

Stull, R. B.: An Introduction to Boundary Layer Meteorology, Kluwer Academic Publishers, The Netherlands, 1988.

Thornton, J. A., Wooldridge, P. J., Cohen, R. C., Martinez, M., Harder, H., Brune, W. H., Williams, E. J., Roberts, J. M., Fehsenfeld, F. C., Hall, S. R., Shetter, R. E., Wert, B. P., and Fried, A.: Ozone production rates as a function of NO_x abundances and HO_x production rates in the Nashville urban plume, J. Geophys. Res.-Atmos., 107, 4146, 2002.

Thornton, J. A., Jaegle, L., and McNeill, V. F.: Assessing known pathways for HO_2 loss in aqueous atmospheric aerosols: Regional and global impacts on tropospheric oxidants, J. Geophys. Res., 113, 113, D05303, doi:10.1029/2007JD009236, 2008.

Tie, X., Madronich, S., Li, G., Ying, Z., Zhang, R., Garcia, A. R., Lee-Taylor, J., and Liu, Y.: Characterizations of chemical oxidants in Mexico City: A regional chemical dynamical model (WRF-Chem) study, Atmos. Environ., 41, 1989–2008, 2007.

Tressol, M., Ordonez, C., Zbinden, R., Brioude, J., Thouret, V., Mari, C., Nedelec, P., Cammas, J. P., Smit, H., Patz, H. W., and Volz-Thomas, A.: Air pollution during the 2003 European heat wave as seen by MOZAIC airliners, Atmos. Chem. Phys., 8, 2133–2150, 2008, http://www.atmos-chem-phys.net/8/2133/2008/.

UN: World Urbanization Prospects: The 2007 Revision, United Nations, New York, USA, 2008.

Velasco, E., Lamb, B., Westberg, H., Allwine, E., Sosa, G., Arriaga-Colina, J. L., Jobson, B. T., Alexander, M. L., Prazeller, P., Knighton, W. B., Rogers, T. M., Grutter, M., Herndon, S. C., Kolb, C. E., Zavala, M., De Foy, B., Volkamer, R., Molina, L. T., and Molina, M. J.: Distribution, magnitudes, reactivities, ratios and diurnal patterns of volatile organic compounds in the Valley of Mexico during the MCMA 2002 & 2003 field campaigns, Atmos. Chem. Phys., 7, 329–353, 2007, http://www.atmos-chem-phys.net/7/329/2007/.

Volkamer, R., Molina, L. T., Molina, M. J., Shirley, T., and Brune, W. H.: DOAS measurement of glyoxal as an indicator for fast VOC chemistry in urban air, Geophys. Res. Lett., 32, L08806,, doi:10.1029/2005GL022616, 2005.

Volkamer, R., Jimenez, J. L., San Martini, F., Dzepina, K., Zhang, Q., Salcedo, D., Molina, L. T., Worsnop, D. R., and Molina, M. J.: Secondary organic aerosol formation from anthropogenic air pollution: Rapid and higher than expected, Geophys. Res. Lett., 33, L17811, doi:10.1029/2006GL026899, 2006.

Volkamer, R., Sheehy, P., Molina, L., and Molina, M.: Oxidative capacity of the Mexico City atmosphere –Part 1: A radical source perspective, Atmos. Chem. Phys. Discuss., 7, 5365–5412, 2007, http://www.atmos-chem-phys-discuss.net/7/5365/2007/.

Wang, Y. H., Logan, J. A., and Jacob, D. J.: Global simulation of tropospheric O_3-NO_x-hydrocarbon chemistry 2. Model evaluation and global ozone budget, J. Geophys. Res.-Atmospheres, 103, 10727–10755, 1998.

Wesely, M. L. and Hicks, B. B.: A review of the current status of knowledge on dry deposition, Atmos. Environ., 34, 2261–2282, 2000.

Williams, E. J., Baumann, K., Roberts, J. M., Bertman, S. B., Norton, R. B., Fehsenfeld, F. C., Springston, S. R., Nunnermacker, L. J., Newman, L., Olszyna, K., Meagher, J., Hartsell, B., Edgerton, E., Pearson, J. R., and Rodgers, M. O.: Intercomparison of ground-based NO_y measurement techniques, J. Geophys. Res.-Atmos., 103, 22261–22280, 1998.

Wood, E. C., Canagaratna, M., and Herndon, S.: Investigation of the correlation between odd-oxygen and secondary organic aerosol in Mexico City and Houston, in preparation, 2009.

Yauk, C., Polyzos, A., Rowan-Carroll, A., Somers, C. M., Godschalk, R. W., Van Schooten, F. J., Berndt, M. L., Pogribny, I. P., Koturbash, I., Williams, A., Douglas, G. R., and Kovalchuk, O.: Germ-line mutations, DNA damage, and global hypermethylation in mice exposed to particulate air pollution in an urban/industrial location, Proceedings of the National Academy of Science, 105, 605–610, 2008.

Zavala, M., Herndon, S. C., Slott, R. S., Dunlea, E. J., Marr, L. C., Shorter, J. H., Zahniser, M., Knighton, W. B., Rogers, T. M., and Kolb, C. E.: Characterization of on-road vehicle emissions in the Mexico City Metropolitan Area using a mobile laboratory in chase and fleet average measurement modes during the MCMA-2003 field campaign, Atmos. Chem. Phys., 6, 5129–5142, 2006, http://www.atmos-chem-phys.net/6/5129/2006/.

Zhao, J. and Zhang, R.: Proton transfer reaction rate constants between hydronium ion (H3O+) and volatile organic compounds (VOCs), Atmos. Environ., 38, 2177–2185, 2004.

Zheng, J., Zhang, R., Fortner, E. C., Volkamer, R. M., Molina, L., Aiken, A. C., Jimenez, J. L., Gaggeler, K., Dommen, J., Dusanter, S., Stevens, P. S., and Tie, X.: Measurements of HNO_3 and N_2O_5 using Ion drift – Chemical Ionization Mass Spectrometry during the MCMA – 2006 Campaign, Atmos. Chem. Phys., 8, 6823–6838, 2008, http://www.atmos-chem-phys.net/8/6823/2008/.